

# Fabrication and optimization of 3D metallic parts using electroplating of additively manufactured parts

Panteha Fallah

A Thesis  
In  
The Department  
Of  
Mechanical and Industrial Engineering

Presented in Partial Fulfillment of the Requirements  
for the Degree of Master of Applied Science (Mechanical Engineering) at  
Concordia University  
Montreal, Quebec, Canada

Summer 2018

©Panteha Fallah, 2018

CONCORDIA UNIVERSITY  
School of Graduate Studies

This is to certify that the thesis prepared

By: Panteha Fallah

Entitled: Fabrication and optimization of 3D metallic parts using electroplating of additively manufactured parts

and submitted in partial fulfillment of the requirements for the degree of

Master of Applied Science (Mechanical Engineering)

complies with the regulations of the University and meets the accepted standards with respect to originality and quality.

Signed by the final examining committee:

_____	Chair
M. Hojjati	_____ Examiner
A. Visscher	_____ Examiner
T. Kwok	_____ Thesis Supervisor(s)
R. Wuthrich	_____

Approved by \_\_\_\_\_  
Chair of Department or Graduate Program Director

\_\_\_\_\_  
Dean,

Date \_\_\_\_\_

# **ABSTRACT**

Fabrication and optimization of 3D metallic parts using electroplating of additively manufactured part

Panteha Fallah

Additive manufacturing (AM) technologies can be used to manufacture metallic and non-metallic parts. Combination of electrochemistry and additive manufacturing technology makes possible the fabrication of different shapes and geometrical features with very smooth surfaces.

In this thesis, an overview of the basics of electroless copper plating, copper electroplating, AM technologies and their applications are covered. An introduction to how an AM part is produced, how electroless copper plating is carried out on a non-conductive surface, how an electroless copper plated part can be electroformed, how to obtain sufficient thickness of the copper coating while keeping the surface smooth have been shown.

FDM (fused deposition modeling) technology is used to print a 3D ABS (Acrylonitrile butadiene styrene) part due to its low manufacturing cost and a minimal amount of waste material. Then, a produced ABS part got conductive through electroless copper plating process enabling the electroplating afterward.

Optimal parameters of electroless copper plating and copper electroplating (in three different modes: galvanostatic, potentiostatic and pulse-potentiostatic) on a planar geometry are achieved with the goal of obtaining a smooth surface.

The results show that the surface roughness of a produced 3D metallic part can be significantly lowered using pulse electrodeposition. Although the presence of additives in the solution can affect the surface roughness and properties of the deposit, using pulse electroplating technique is offered as an alternative to the additives which are almost toxic, and add impurities within copper deposit.

## **Acknowledgments**

I would like to express my gratitude to my thesis supervisor Dr. Rolf Wuthrich for all his useful advice and continuous support. His discipline to work and expertise in electrochemistry has provided me with an excellent basis to work during this endeavor. It has been my great honor and privilege to work under his supervision.

Special thanks to Mr. Lucas Hof who assisted me a lot with my research and his generous and knowledgeable suggestions. Also, I would like to thank my colleagues, Rahul Singh, Jaimin Panchal and Zahra Chaqazardi who helped me with their experience and knowledge.

I want to express my deepest gratitude to my loving husband, my supportive parents and my one and only sister. You have been very important for me to go through this long journey. With all my love, I dedicate this thesis to you. Dear parents, this thesis is the result of your example of hardworking to overcome all obstacles and materialize my dreams. No matter the distance, you and my sister have always been on my mind and my heart. My beloved Ali, all our efforts and sacrifices have finally been compensated with this achievement. Thank you for your company, encouragement and for being my inspiration.

# Contents

ABSTRACT.....	iii
Acknowledgments.....	v
1. Introduction and literature review .....	1
1.1. Electroless plating process .....	3
1.1.1. Electroless copper plating of plastics.....	5
1.2. Copper Electrodeposition.....	6
1.2.1. Electrode-Electrolyte interface .....	7
1.2.2. Concepts of pulse electroplating techniques.....	11
1.3. An overview of additive manufacturing techniques .....	15
1.3.1. The classifications of AM processes.....	16
1.3.2. Advantages and limitations of AM processes.....	18
1.3.3. Applications .....	19
2. Experimental procedures .....	21
2.1. Substrate preparation.....	21
2.2. Preparation of Copper deposition electrolyte and Electrochemical cell .....	22
2.3. Polarization curve using a rotary disk electrode (RDE) and in-house developed ECTK software .....	24
2.4. Electroplating process .....	26
2.4.1. Galvanostatic mode.....	26
2.4.2. Potentiostatic mode.....	27
2.4.3. Pulse potentiostatic mode .....	27
2.5. Coatings characterization .....	28
2.5.1. Coating thickness and mass measurement.....	28
2.5.2. Coating surface roughness measurement.....	28
2.5.3. Scanning Electron Microscopy (SEM).....	29
2.6. 3D printing of an ABS part .....	29
2.6.1. Surface roughness measurement of an ABS part.....	29
2.7. Copper electroless plating of an ABS printed part.....	30
2.7.1. Surface resistance and roughness measurement .....	32
2.8. Copper electroplating of electroless copper plated ABS part .....	32

2.8.1.	Surface roughness measurement.....	32
3.	Results and discussion.....	33
3.1.	Potentiostatic plating mode.....	33
3.1.1.	Polarization curves of two different electrolyte concentrations.....	33
3.1.2.	The effect of different potentials on surface roughness of the deposits at an identical charge of 0.13 C/mm <sup>2</sup> .....	35
3.1.3.	The effect of different potentials on coatings morphology at an identical charge of 0.13 C/mm <sup>2</sup> .....	38
3.1.4.	The effect of charge on thickness and surface roughness of the coatings at a potential of -150 mV.....	41
3.1.5.	The effect of quantity of electricity on coatings morphology at a potential of -150 mV	44
3.2.	Galvanostatic plating mode.....	46
3.2.1.	The effect of charge on the thickness and surface roughness of the coatings at a current density of 5 mA/cm <sup>2</sup> .....	46
3.2.2.	The effect of quantity of electricity on coatings morphology for a current density of 5 mA/cm <sup>2</sup> .....	49
3.3.	Pulse-potentiostatic plating mode.....	52
3.3.1.	The effect of total charge on thickness and surface roughness of the coatings obtained by pulse potentiostatic plating.....	56
3.3.2.	The effect of quantity of electricity on the morphology of the pulse plated coatings (polishing pulse charge is 10% of the depositing pulse charge).....	60
3.4.	Comparison of galvanostatic, potentiostatic and pulse-potentiostatic copper plating ...	62
3.5.	Electroless copper plated ABS printed part.....	64
3.5.1.	Surface roughness and resistance measurements.....	65
3.6.	Copper electroforming of ABS printed part in galvanostatic, potentiostatic and pulse-potentiostatic modes.....	66
3.6.1.	Surface roughness measurements.....	67
3.7.	Applications.....	70
4.	Conclusion and future work.....	73
	References.....	75

## List of Figures

Figure 1-1. Comparison of Thickness vs. Time of electroless plating between immersion and electroless plating [10].....	4
Figure 1-2. schematic of copper deposition from an aqueous acid copper sulfate .....	7
Figure 1-3. Helmholtz-Perrin model of the electrical double-layer [18].....	8
Figure 1-4. Metal ion concentration profile as a function of distance from the surface [18] .....	9
Figure 1-5. Four regions in the general current–overpotential relationship: 1, linear; 2, exponential; 3, mixed control; 4, limiting current density region [11].....	10
Figure 1-6. Schematic concentration profile at the cathode for pulse plating conditions: $\delta_p$ , pulsating diffusion layer thickness; $\delta_s$ , stationary diffusion layer thickness; $\delta_N$ , Nernst diffusion layer thickness [11].....	12
Figure 1-7. Two major waveforms used in pulse technique, $t_{on}$ : the on period of a cycle, $t_{off}$ : the off period of a cycle, $\lambda$ : the cycle time [21][11][22].....	12
Figure 1-8. 3D printing process [39].....	15
Figure 1-9. Additive vs. subtractive manufacturing [39].....	16
Table 1-1. Summary of 3D printing methods [39] .....	17
Figure 1-10. Schematic diagram of fused deposition modeling (FDM) [39] .....	18
Figure 2-1. Surface roughness measurement of the copper substrate after preparation obtained by confocal laser microscopy.....	22
Figure 2-2. Electrolyte preparation .....	23
Figure 2-3. Electrochemical cell.....	23
Figure 2-4. Experimental system .....	24
Figure 2-5. Rotary disk electrode compartments assembling and ECTK script.....	25
Figure 2-6. Potentiostat/Galvanostat.....	26
Figure 2-7. Schematic diagram of the pulse potentiostatic electroplating cycles.....	27
Figure 2-8. Coating thickness measurement using a micrometer .....	28
Figure 2-9. The determined location for surface roughness measurement.....	30
Table 2-1. Electroless plating condition for ABS 3D parts .....	30
Figure 2-10. Electroless plating steps; a) Degreasing b) Etching c) Activation d) Reduction e) Electroless deposition .....	31
Figure 2-11. Left: ABS printed part, Middle: Electroless copper plated ABS part, Right: Copper electroforming of electroless copper plated part.....	32
Figure 3-1. Polarization curves for the cathodic process of copper deposition from 0.15 M.....	34
CuSO <sub>4</sub> in 0.50 M H <sub>2</sub> SO <sub>4</sub> versus Cu at different angular velocities (100, 300 and 1000 rpm) ...	34

Figure 3-2. Polarization curve for the cathodic process of copper deposition from 0.5 M $\text{CuSO}_4$ in 1 M $\text{H}_2\text{SO}_4$ .....	35
Figure 3-3. The effect of varying potential on the deposits color for the constant given charge (the applied potential from right to left is -150, -200, -350, -400, -500, -750 and -825 mV).....	36
Figure 3-4. 3D maps of the morphology of the coatings obtained by confocal laser microscopy: a) -150 mV, b) -200 mV, c) -350 mV, d) -400 mV, e) -500 mV, f) -750 mV, g) -825 mV .....	37
Figure 3-5. The effect of different potentials on the surface roughness of the deposits at an identical charge of $0.13 \text{ C/mm}^2$ .....	38
Figure 3-6. Copper deposits obtained at potentials of a) -150mV b) -350mV c) -400mV d) -750mV e) -825 mV. Magnification: X5000, quantity of electricity: $0.13 \text{ C/mm}^2$ .....	39
Figure 3-7. The effect of varying total charge on the thickness of the deposits for a given potential of -150mV vs. Cu. Line drawn according to faraday's law (Eq 3-1) .....	41
Figure 3-8. The 3D maps of the morphology of the coatings obtained by confocal laser microscopy at potential of -150mV for different charges a) $0.13\text{C/mm}^2$ b) $0.33\text{C/mm}^2$ c) $1\text{C/mm}^2$ d) $1.33\text{C/mm}^2$ e) $3.33\text{C/mm}^2$ f) $8.33\text{C/mm}^2$ g) $10\text{C/mm}^2$ h) $13.33\text{C/mm}^2$ .....	43
Figure 3-9. The effect of quantity of electricity on surface roughness at a deposition potential of -150 mV .....	43
Figure 3-10. The SEM micrographs of the coatings obtained at different quantity of electricity at a potential of -150mV. a) $0.33\text{C/mm}^2$ X2000 b) $1.33 \text{ C/mm}^2$ X2000 c) $3.33 \text{ C/mm}^2$ X2000 d) $8.33\text{C/mm}^2$ X2000 e) $10\text{C/mm}^2$ X1000 f) $13.33\text{C/mm}^2$ X1000 .....	45
Figure 3-11. The surface roughness of the coatings in function of current density for a constant charge ( $0.33 \text{ C/mm}^2$ ).....	46
Figure 3-12. The effect of varying total charge on the thickness of the deposits for a given current density of $5\text{mA/cm}^2$ .....	47
Figure 3-13. The 3D maps of the morphology of the coatings obtained by confocal laser microscopy at a current density of $5\text{mA/Cm}^2$ for different charges a) $1.33\text{C/mm}^2$ b) $3.33\text{C/mm}^2$ c) $8.33\text{C/mm}^2$ d) $10\text{C/mm}^2$ .....	48
Figure 3-14. The effect of quantity of electricity on surface roughness at a current density of $5\text{mA/Cm}^2$ .....	49
Figure 3-15. The SEM micrographs of the coatings obtained at different quantity of electricity at current density of $5\text{mA/Cm}^2$ . a) $1.33\text{C/mm}^2$ X2000 b) $3.33\text{C/mm}^2$ X2000 c) $8.33\text{C/mm}^2$ X2000 d) $10\text{C/mm}^2$ X2000 .....	50
Figure 3-16. schematic representation of an E(t) relationship for a constant current density of $5\text{mA/cm}^2$ for a quantity of electricity of $8.33 \text{ C/mm}^2$ .....	51
Figure 3-17. The schematic of I-t of the initial cycles contains $0.013 \text{ C/mm}^2$ cathodic charge and $0.0013 \text{ C/mm}^2$ anodic charge (the corresponding potentials are -150 mV and +100mV vs Cu) .	53
Figure 3-18. a) The influence of the number of cycles on the cathodic current for 832 total number of cycles. b) The effect of the number of cycles on the cathodic pulse duration for the 832 total number of cycles.....	54

Figure 3-19. a) The influence of the number of cycles on the anodic current for 832 total number of cycles. b) The effect of the number of cycles on the anodic pulse duration for the 832 total number of cycles.....	55
Figure 3-20. The effect of varying total charge on mass of the 10% polished deposits (the cathodic charge: 0.013 C/mm <sup>2</sup> , the anodic charge: 0.0013 C/mm <sup>2</sup> , the cathodic potential: -150 mV, the anodic potential: +100 mV) .....	56
Figure 3-21. The effect of different anodic charge (1%, 10% and 30% of cathodic charge) on the mass of the deposits by keeping the cathodic charge constant at 0.013 C/mm <sup>2</sup> for the total charge of 13.8 C/mm <sup>2</sup> .....	57
Figure 3-22. The 3D maps of the morphology of the 10% polished coatings obtained by confocal laser microscopy at certain pulse parameters (4C at -150mV for deposition and 0.4C at +100mV for polishing) for different total charges: a)0.24 C/mm <sup>2</sup> b)0.6 C/mm <sup>2</sup> c)2.4 C/mm <sup>2</sup> d)7.2 C/mm <sup>2</sup> e)10.83 C/mm <sup>2</sup> .....	58
Figure 3-23. The effect of quantity of electricity on surface roughness of the 10% polished deposits. Freely drawn trendline. ....	59
Figure 3-24. The effect of different anodic charge (1%, 10% and 30% of cathodic charge) on the surface roughness of the deposits by keeping the cathodic charge constant at 0.013 C/mm <sup>2</sup> for the total charge of 13.8 C/mm <sup>2</sup> .....	59
Figure 3-25. The SEM micrographs of the pulse plated coatings obtained at the different total quantity of electricity. a)0.24 C/mm <sup>2</sup> X2000 b)0.6 C/mm <sup>2</sup> X2000 c)2.4 C/mm <sup>2</sup> X2000 d)7.2 C/mm <sup>2</sup> X2000 .....	61
Figure 3-26. The schematic of difference in surface roughness of the copper deposits in function of charge for galvanostatic, potentiostatic and pulse-potentiostatic plating modes.....	62
Figure 3-27. Copper deposits made by potentiostatic plating and pulse-potentiostatic plating modes from left to right, for the same charge of 10 C/mm <sup>2</sup> .....	64
Figure 3-28. a) ABS printed part b) Electroless plated ABS part.....	64
Figure 3-29. The 2D and 3D maps of the ABS part obtained by confocal laser microscopy.....	65
Figure 3-30. The 3D map of the electroless copper plated ABS part.....	66
Figure 3-31. Copper electroforming of a non-conductive 3D printed ABS part <b>Above</b> ) Right to left: Galvanostatic copper electroformed part, potentiostatic copper electroformed part, pulse-potentiostatic copper electroformed part <b>Below</b> ) View from inside the hollow part .....	67
Figure 3-32. 3D maps of the morphology of the copper electroplated ABS part in three conditions: a) Galvanostatic b) Potentiostatic c) Pulse-reverse electroplating.....	68
Figure 3-33. Surface roughness comparison of AM part created by different electroplating modes .....	69
Figure 3-34. Copper electroformed plaster part (potentiostatic mode,- 0.3V applied potential)..	70
Figure 3-35. Copper electroformed plaster part.....	70
Figure 3-36. Process flow from 3D printing a non-conductive ABS part up to electroplating (Cu) the copper painted part.....	71

Figure 3-37. Copper electroforming of a SLA printed part (electronic chips) ..... 71  
Figure 3-38. An example of fabrication of an electrode used in electropolishing..... 72

**List of tables**

Table 1-1. Summary of 3D printing methods [39] ..... 17  
Table 2-1. Electroless plating condition for ABS 3D parts ..... 30

# 1. Introduction and literature review

Advances in Additive Manufacturing (AM) allow for high-resolution fabrication of complex three-dimensional structures which enables the fabrication of tailored workpieces with virtually any shape. Promising applications for this approach are the development of lattices for orthopedic bone implants, cooling channels inside molds for casting and lightweight parts for the aerospace industry.

However, AM has its own limitations. Currently, significant issues are the limited materials available for metal printing, limited quality in surface finish and the challenge in printing fine features (typically below few hundred microns thick features).

In this work, to address the issue of printing thin features, we propose a novel approach to produce thin and light metallic parts of complex shapes. The process starts by printing a plastic part (ABS part) which is subsequently made conductive by electroless copper plating. Copper electroforming is carried out afterwards. Dissolving the plastic part allows in the last step the creation of self-standing ultra-light metal parts with a high-quality surface finish and high complexity. Several applications can benefit from a technology able to produce complex metal parts with thin features like watch industry, medical devices or aerospace and space applications where weight plays a key factor.

Surface roughness is a significant factor in the above-mentioned applications. AM technology is not able to produce a part with satisfactory surface roughness since the size of the used powders (metallic particles) are typically 25 microns or higher in diameter, and the fact that a few layers are needed before a stable structure can be achieved resulting in staircase effect and presence of semi-melted beads on the surface.

There are two ways to achieve good surface quality in electrodeposition which are the use of pulse plating and additives in the plating bath. Pulse current (PC) plating is known to improve the morphology and properties of deposits in the absence of additives [1][2].

Deposit properties (brightness, smoothness, and microhardness) can also be improved by adding additives in a sulfate-plating bath since they cause leveling effect and are used as a brightening agent. However, the usage of additives in the plating baths usually results in the following three drawbacks.

First, the impurity levels within Cu deposits will be significantly increased since the intercalation of additives into the Cu deposit may change its textural properties, e.g., electronic conductivity, grain size, crystalline structure, etc. Second, the control and monitor of the plating baths with additives is relatively difficult during the electroplating. Third, plating baths with additives are likely commercially uncompetitive compared to their counterparts without additives, due to the cost and environmental considerations. Hence, it is more desirable to develop plating bath without any additives [3][4][5].

In the proposed study, the effect of pulse plating on surface roughness of the coating and how a 3D metallic AM part with a thin thickness is produced is carried out.

## 1.1. Electroless plating process

Electroless plating is a chemical method of plating metals from an aqueous solution without the use of electrical power [6].

Electroless plating is a method to achieve a thin metallic film on metals, plastics or ceramics which is usually applied for metallization of non-conductive parts for the subsequent plating [7].

The metallization of plastics has a variety of applications such as the fabrication of printed circuits in microelectronics and decorative coatings in general manufacturing [8]. Also, it is used to metalize multi-walled carbon nanotubes to not only maintain its excellent performance but also increase the surface active sites [9].

Metal displacement reaction happens when a metal substrate is immersed in a solution. The metal atoms of the substrate dissolve in the solution and are replaced by the atoms from the solution. The displacement reaction lasts until the whole surface of the substrate is covered by the atoms from the solution. At this point, the dissolution stops and deposition ceases. This process, called immersion plating, allows deposition of a few microns, usually 1 to 3 microns.

To build a thick deposit, a sustainable oxidation reaction (reducing agent) should be employed as an alternative to the dissolution of the substrate which is called electroless plating. Figure 1-1 shows the difference in thickness vs. time between immersion plating and electroless plating [10].

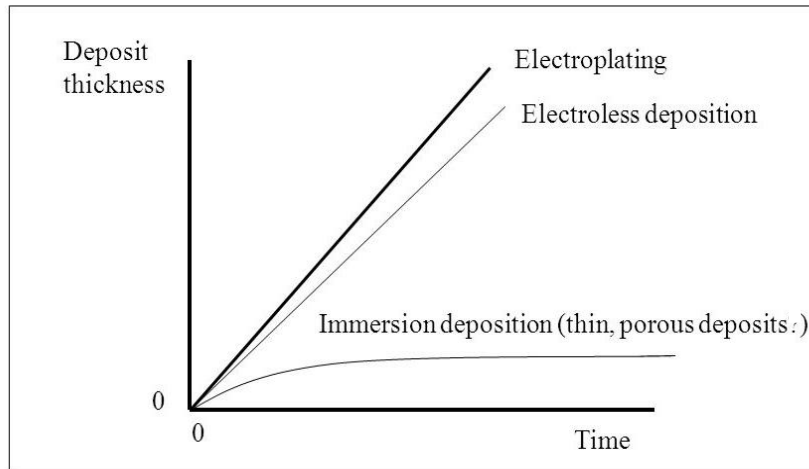


*Figure 1-1. Comparison of Thickness vs. Time of electroless plating between immersion and electroless plating [10].*

Electroless plating bath contains a source of metal ions, reducing agent, complexant, buffer, exultant and stabilizer. To avoid the dissolution of the substrate, the redox potential for the reducing agent should be more negative than the metal being plated.

Complexants are added to maintain the metal ions and prevent precipitation of metal in bulk. Also, the pH of the solution changes during plating and could affect the deposition rate and properties. Buffers are added to stabilize the pH.

The electroless plating bath is unstable in which active nuclei like dust and metallic particles can decompose the plating bath. Stabilizers shield active nuclei from reducing agent.

Sometimes the plating rate is depressed by the additional use of complexants. Exaltant can increase the deposition rate to an acceptable level without causing bath instability [11].

### 1.1.1. Electroless copper plating of plastics

Automotive, appliance, hardware parts, circuit boards and through-hole plating, represent significant markets for electroless copper. In through-hole plating of circuit boards, the use of electroless copper provides excellent electrical conductivity and uniform thickness in these hard-to-reach areas [6].

Electroless plating on plastics requires pre-treatment steps before plating to form catalytic nuclei on the surface to initiate electroless deposition. The preparation steps include cleaning, etching, activation and reduction [12].

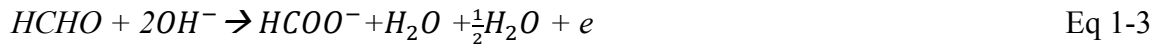
Components of electroless copper deposition contain a source of metal ions, reducing agent and complexant. The best-known reducing agent for electroless copper deposition is formaldehyde (HCHO) [10].

The total reaction of deposition in the presence of formaldehyde (reducing agent) whose oxidation is accompanied by hydrogen evolution is: [13][11]



Formic acid ( $HCOO^-$ ) is the oxidation product of a reducing agent.

The overall reaction is the result of two partial reactions, cathodic partial reaction, and the anodic partial reaction, given by Eq 1-2 and 1-3, respectively.



These reactions happen at the metal-solution interphase. Each reaction strives to establish its own equilibrium potential,  $E_{eq}$ , resulting in the creation of a *steady-state mixed potential*,  $E_{mp}$  [11].

## 1.2. Copper Electrodeposition

Copper has become an alternative to aluminum as an interconnection material and has many engineering and decorative applications, due to its unique properties: i. Toughness; ii. Ductility; iii. Resistance to many corrosive environments; iv. High electrical conductivity and v. high thermal conductivity [14][15][16].

Copper can be deposited by different methods such as physical vapor deposition (PVD) and chemical vapor deposition (CVD). However, a simpler way is electroplating which is a low cost and low-temperature process and also has excellent coverage on irregularly shaped parts [16].

One of the significant uses of deposition of copper is electroforming [11].

Electroplating is an electrochemical process in which cathodic and anodic reactions occur at the same time on the cathode and anode surfaces by passing the electric current in which the reaction in an aqueous medium at the cathode follows the equation:  $M^{n+} + ne^- \rightarrow M$ , with a similar anode reaction. The anode material can be either a sacrificial anode or an inert anode. For the sacrificial anode, the anode reaction is  $M \rightarrow M^{n+} + ne^-$ .

There are different types of plating baths used to electrodeposit copper which include acid copper, cyanide copper, and pyrophosphate systems [11]. Acid copper bath is the most common system

used for copper electrodeposition. The present study will focus on sulfate-based acid copper electrodeposition.

Figure 1-2 shows the schematic of copper deposition from an aqueous acid copper sulfate.

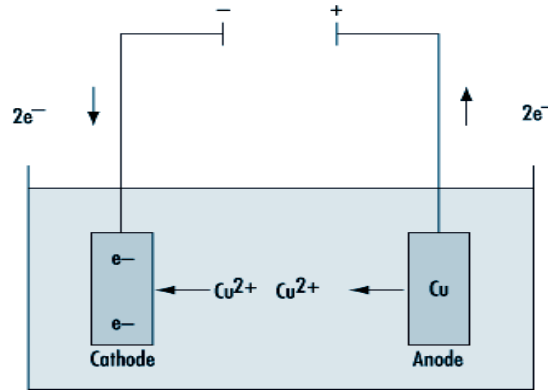


*Figure 1-2. schematic of copper deposition from an aqueous acid copper sulfate*

### 1.2.1. Electrode-Electrolyte interface

A three-electrode electroplating system is composed of a cathode (working electrode), an anode (counter electrode) and a reference electrode. When the system is connected to the power source, current flows through the system. When a work piece is immersed in an electrolyte, the electrode potential of the working electrode is always measured with respect to the reference electrode.

#### 1.2.1.1. Double layer

As soon as a metal is immersed in the electrolyte, an electrically charged layer forms at the electrode-electrolyte interface. At this time, a potential is generated due to the unequal distribution

of charge along the interface. This interface capacitance has been named the ‘double layer’. According to the Helmholtz-Perrin model, electrons on the working electrode and metal ions in electrolyte side, co-exist in equal measure at the interface. It is shown in Figure 1-3 that the potential gradient within the Helmholtz layer is linear [17][18][19].

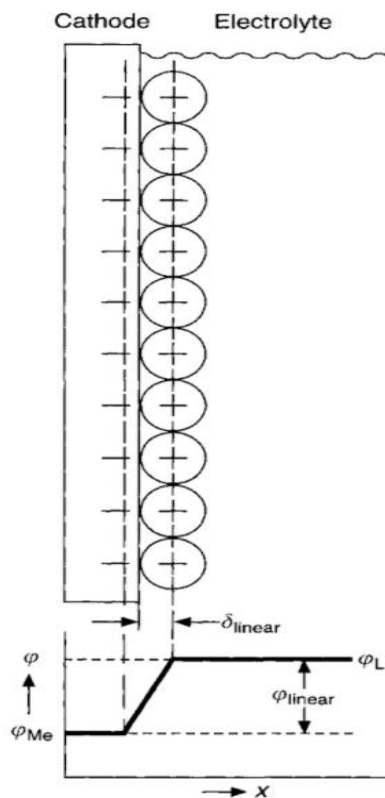


Figure 1-3. Helmholtz-Perrin model of the electrical double-layer [18]

### 1.2.1.2. Mass transport and rotating disk electrode

When a voltage is applied between two electrodes in an electrochemical cell, the current will pass through the external circuit carrying the electrons. The anode will dissolve, and cations are moving towards the cathode and anions present in the solution will migrate to the anode. These movements of ions cause the ionic current in the electrolyte.

There are three mechanisms of ions movements to the electrode surfaces; migration, diffusion, and convection.

In migration mechanism, the motion of a charge caused by the potential gradient. Convective mass transport results from the movement of a bulk solution such as stirring or density gradient (natural convection) caused by thermal effects.

The driving force for the diffusion of species is the concentration gradient (formally chemical potential) [18].

Figure 1-4 shows the concentration-depth profile indicating the depletion of reactants at the electrode surface. Nernst diffusion layer is a region in the vicinity of the electrode where the concentration is different from the concentration in the bulk solution.

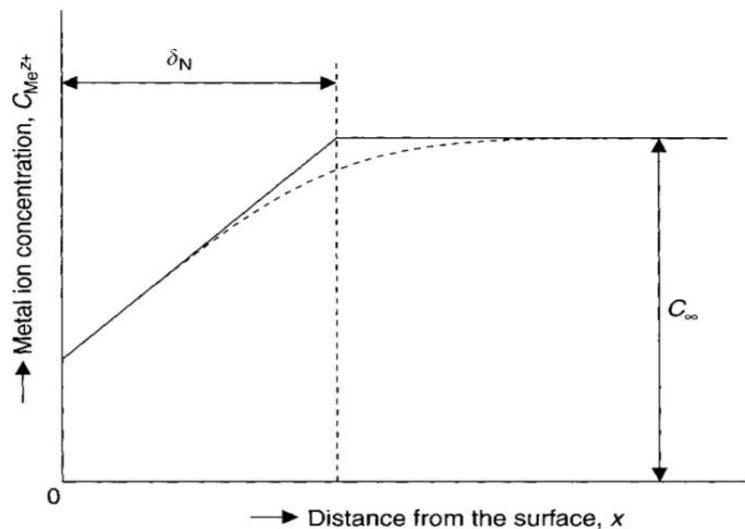


Figure 1-4. Metal ion concentration profile as a function of distance from the surface [18]

The current-potential relationship is shown in Figure 1-5. This relationship has a plateau where the deposition reaction rate is limited by transport of metallic ions ( $M^+$ ) in the solution. The limiting current density is given by [11][20]:

From Fick's first law:

$$j = nFJ \text{ (J is the flux of electroactive material at the surface)} \quad \text{Eq 1-4}$$

$$j = nFD \left( \frac{\partial c}{\partial x} \right)_{x=0} = nFD \frac{c^0 - c^s}{\delta N} \quad \text{Eq 1-5}$$

( $c^0$  is the bulk concentration of ions,  $c^s$  is the electrode surface concentration).

If a sufficiently high overpotential (more cathodic) is selected, the surface concentration decreases to a small value, and the current density is determined by the rate of diffusion. This limiting value is termed the diffusion-limited current density:[20]

$$j_{lim} = nFD \frac{c^0}{\delta N} \quad \text{Eq 1-6}$$

Where  $D$  is the diffusion coefficient of the depositing species,  $\delta$  is the diffusion layer thickness,  $n$  the number of electrons involved in the reaction,  $F$  is the Faraday constant. It should be noted that at the values of limiting current density, the species are reduced as they reach the electrode surface. At this condition, the concentration of the reactant is nil, and the deposition rate is controlled by the rate of transport of the reactant to the electrode.

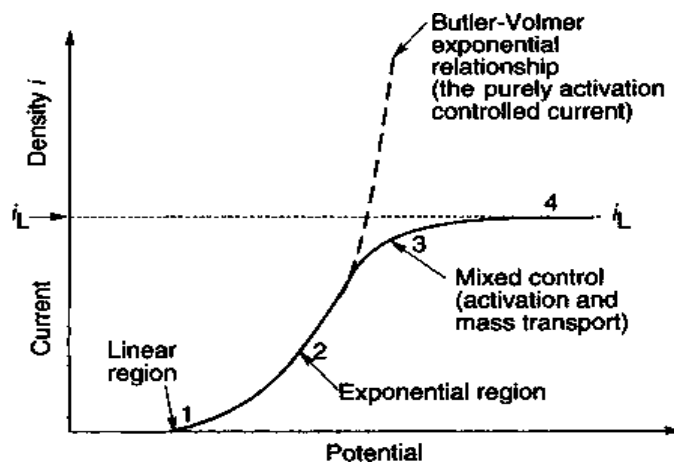


Figure 1-5. Four regions in the general current–overpotential relationship: 1, linear; 2, exponential; 3, mixed control; 4, limiting current density region [11].

According to Figure 1-5, at low potentials, the current follows the Butler-Volmer equation. However, by increasing the potential, there is a transition region where both electron transfer and mass transport rates play a role reaching to the limiting current region where only the mass transport is rate determining [20].

If there is a convective flow near an electrode, as the convection is stronger the value of  $\delta_N$  is smaller. When the flow is laminar, the velocity at the electrode surface is zero. In case of rotating electrode which rotates with an angular velocity ( $\omega$ ) in the solution,  $\delta_N$  and the limiting current density on disk are:

$$\delta_N = 1.61 D^{1/3} \nu^{1/6} \omega^{-1/2} \quad \text{Eq 1-7}$$

$$j_{lim} = 0.62 nFD^{2/3} \nu^{-1/6} \omega^{1/2} c^0 \quad (\text{Levich equation}) \quad \text{Eq 1-8}$$

where  $\nu$  is the kinematic velocity. It is noted that by increasing the angular velocity, limiting current density is increasing.

### 1.2.2. Concepts of pulse electroplating techniques

In the conventional DC plating, there is only one variable parameter, namely current density or potential.

Modification of the diffusion layer is a significant parameter in pulse deposition technique in which the Nernst diffusion layer is split into two diffusion layers: pulsating diffusion layer and the stationary diffusion layer (see Figure 1-6.) [11].

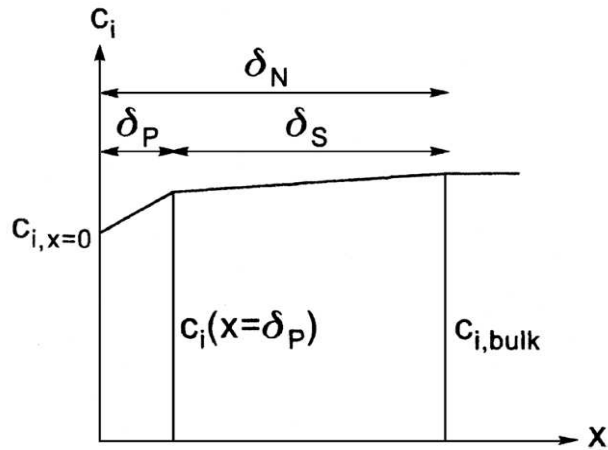


Figure 1-6. Schematic concentration profile at the cathode for pulse plating conditions:  $\delta_p$ , pulsating diffusion layer thickness;  $\delta_s$ , stationary diffusion layer thickness;  $\delta_N$ , Nernst diffusion layer thickness [11]

The two major waveforms that are used in pulse technique are shown in Figure 1-7: rectangular pulse deposition technique (unipolar) and the periodic reverse deposition (bipolar) [21][11].

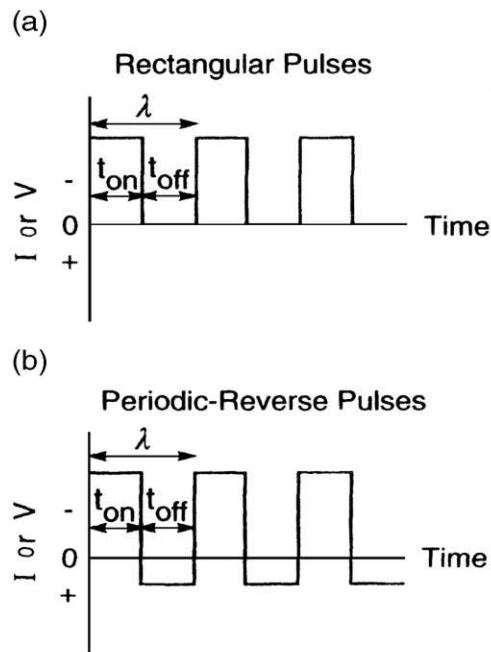


Figure 1-7. Two major waveforms used in pulse technique,  $t_{on}$ : the on period of a cycle,  $t_{off}$ : the off period of a cycle,  $\lambda$ : the cycle time [21][11][22]

In pulse electroplating, the potential/current is alternated between two different values. Each pulse contains an on-time and an off-time in which the current/potential is applied during  $T_{on}$ , and the zero current is applied during  $T_{off}$  [21][11].

In reverse pulse deposition, the current or potential is periodically swapped from the anodic to the cathodic polarization ( $t_c$ : cathodic pulse period,  $t_a$ : anodic pulse period) [11].

### 1.2.2.1. Pulse and pulse reverse electroplating parameters

There are various parameters that can be varied in pulse deposition technique, (i) on-time, (ii) off-time, and (iii) peak current density.

The duty cycle ( $\gamma$ ) corresponds to the percentage of total time of a cycle and is given by:

$$\gamma = \frac{T_{on}}{T_{on}+T_{off}} = Tonf \quad \text{Eq 1-9}$$

where  $f$  is frequency, defined as the reciprocal of the cycle time:

$$f = \frac{1}{T_{on}+T_{off}} = 1/T \quad \text{Eq 1-10}$$

In pulse reverse deposition, the duty cycle is given by:

$$\gamma = Tc/(Ta + Tc) \quad \text{Eq 1-11}$$

Where  $T_c$  is the cathodic time, and  $T_a$  is the anodic time of the pulse [23][21][24].

### 1.2.2.2. Pulse and pulse reverse electroplating mechanisms

In DC plating, a charged layer is formed around the cathode which prevents the ions from reaching the cathode surface. However, in pulse plating,  $T_{\text{off}}$  makes this layer to discharge, and the ions migrate to the depleted area. When  $T_{\text{on}}$  happens, more distributed ions are existing for the deposition [21].

In reverse pulse plating, the whole quantity of electricity is not consumed in the formation of the deposit. During the reversal pulse, a part of a deposited layer is dissolved which allows preferential redissolution of dendrites that might have grown during the cathodic pulses. That is why the current efficiency or the rate of metal deposition is decreased in reverse pulse plating compared to DC plating.

Consequently, the amount of electricity flowing through  $T_c$ , must be greater than the quantity of electricity flowing during  $T_a$  [22][25].

In DC plating, crystal growth happens during plating, however pulse plating favours the nucleation of new crystals instead of crystal growth resulting in a smooth, fine grained, less porous, less stress, harder and more compact deposit[26][27][28] in which the physical and mechanical properties of the deposit can be controlled under pulse deposition condition [29][21][30].

Popov and co-workers have found out that smoother and less porous deposits can be obtained by pulse plating than by DC plating [27].

The DC deposition occurs at a current efficiency very close to 100% [27][21].

### 1.3. An overview of additive manufacturing techniques

In the past thirty years, additive manufacturing started to develop from the 1980s [31].

Additive manufacturing (AM) is the *“The process of joining materials to make objects from 3D model data, usually layer upon layer, as opposed to subtractive manufacturing technologies.”*

[32][33][34] which is also known as rapid manufacturing or rapid prototyping [35][33][36].

AM processes include three basic steps (1) design a 3D model and converting to a standard AM file format, (2) the file is sent to an AM machine, (3) a 3D part is built layer by layer (see Figure 1-8)[33]. CAD software is usually used to design a 3D model [37][38].

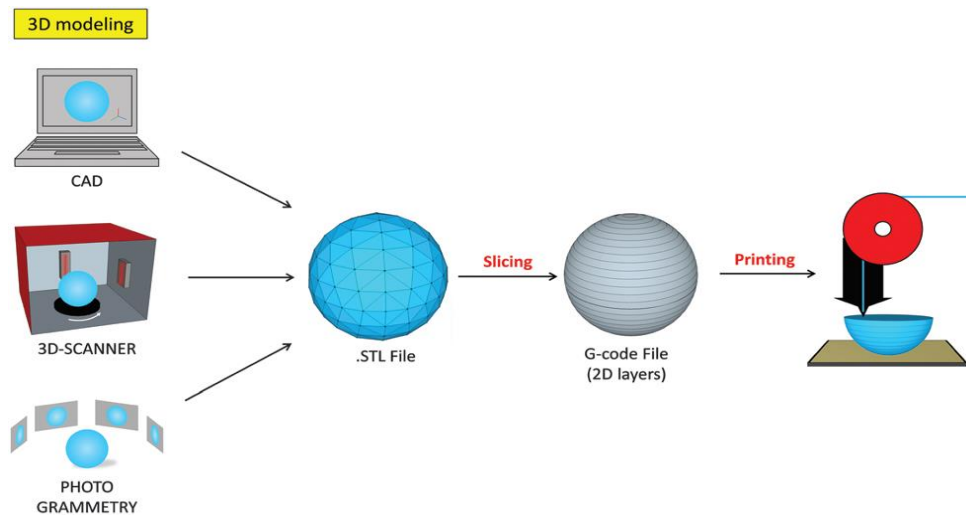
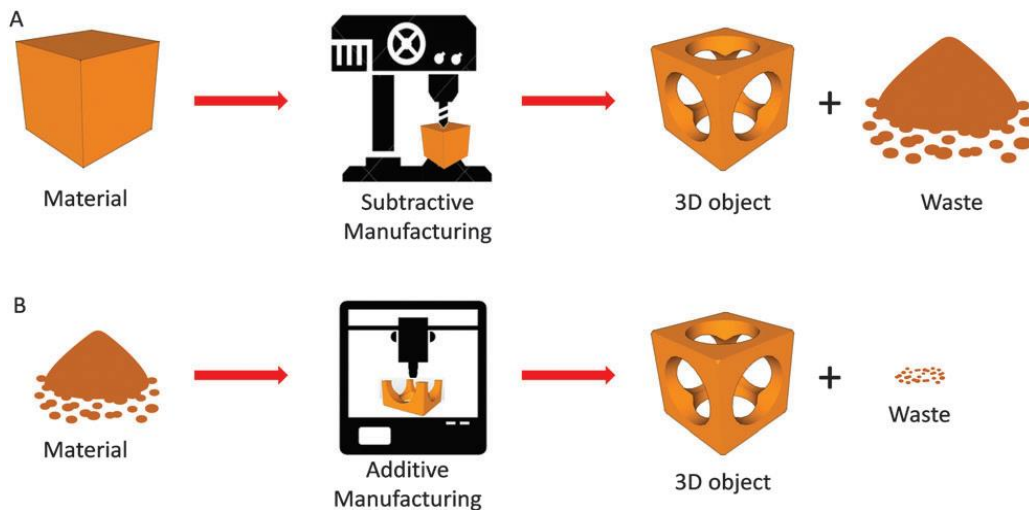


Figure 1-8. 3D printing process [39]

According to Figure 1-8, a 3D model is obtained using CAD software, a 3D scanner or a photogrammetry procedure. Then the 3D design is converted to the STL format at which slicing process is applied using a printer software to obtain a G-code file containing the information of a series of 2D layers. Finally, the printer starts depositing the material layer by layer according to the G-code file [39].

Unlike conventional manufacturing methods, such as machining, drilling, and stamping that produce products by removing materials from a block of material or sheet metal, additive manufacturing produces the final shape by depositing the required amount of material in layer by layer style.

AM process has the capability of making efficient use of raw materials and produce a minimal amount of waste while reaching satisfactory geometric precision (see Figure 1-9) [32][33][39][40][34].



*Figure 1-9. Additive vs. subtractive manufacturing [39]*

### 1.3.1. The classifications of AM processes

Several 3D-printing technologies have been invented. They can be categorized into four main classes based on their particular mechanism: (1) photopolymerization; (2) extrusion; (3) powder based; and (4) lamination [39].

Table 1-1 shows a summary of 3D printing methods.

*Table 1-1. Summary of 3D printing methods [39]*

3D-printing process	Technique	Materials	Advantages	Limitations
Photopolymerization	Stereolithography (SLA)	Photopolymers	Simple	Single material
	Material jetting	Photopolymers	Multimaterial structures	High cost
	Continuous liquid interface printing (CLIP)	UV-curable resins	High speed	Single material
	Two-photon polymerization (2PP)	UV-curable resins	Sub-100 nm resolution	Low yield of production
Extrusion	Fused deposition modeling (FDM)	Thermoplastics (ABS, PLA, PC, PA, <i>etc.</i> ); glass (new); metal (new)	Simple, multimaterial structures; low cost (for thermoplastic materials)	High cost (for glass and metal)
	Robocasting (DIW)	Plastics, ceramic, food, living cells, composites	Versatile	Requires post-processing; low resolution
Powder based	Selective laser sintering (SLS)	Thermoplastics, metals	No need for support material	Limited mechanical properties of object; high cost
	Selective laser melting (SLM)	Metals	No need for support material	High cost
	Electron beam melting (EBM)	Metals	No need for support material	High cost
	Binder jetting	Any material in particulate form	No need for support material; versatile; lower cost than laser-based methods	Limited mechanical properties
	Selective inhibition sintering (SIS)/inhibitor jetting	Metal	Sintering is performed only once after printing; lower cost than laser-based methods	Low resolution; limited mechanical properties
Lamination	Laminated object manufacturing (LOM)	Paper, metal, plastic, <i>etc.</i> as laminated sheets	Versatile	Limited mechanical properties; some design limitations

In this project FDM (fused deposition modeling) technique (extrusion process) is used to print 3D ABS parts which are described in the following sentences.

3D printing methods in extrusion process category include the pre-treatment of the material such as liquefaction which is followed by depositing the model material from a nozzle head dispenser.

This technology is known as fused deposition modeling (FDM) invented by Scott Crump in 1989 [41] which generates 3D objects using thermoplastic materials such as polylactic acid (PLA), acrylonitrile butadiene styrene (ABS), polycarbonate (PC), polyamide (PA), *etc.*

In FDM method, 3D objects are produced by heating the thermoplastic materials to their semi-molten state before extrusion at the dispenser nozzle. Once the deposition happens, the material is solidified making a hard layer sticks at the top of the previous layer. Different nozzles and varying

materials can be used simultaneously during the single printing process to make the multi-material structure (see Figure 1-10) [39].

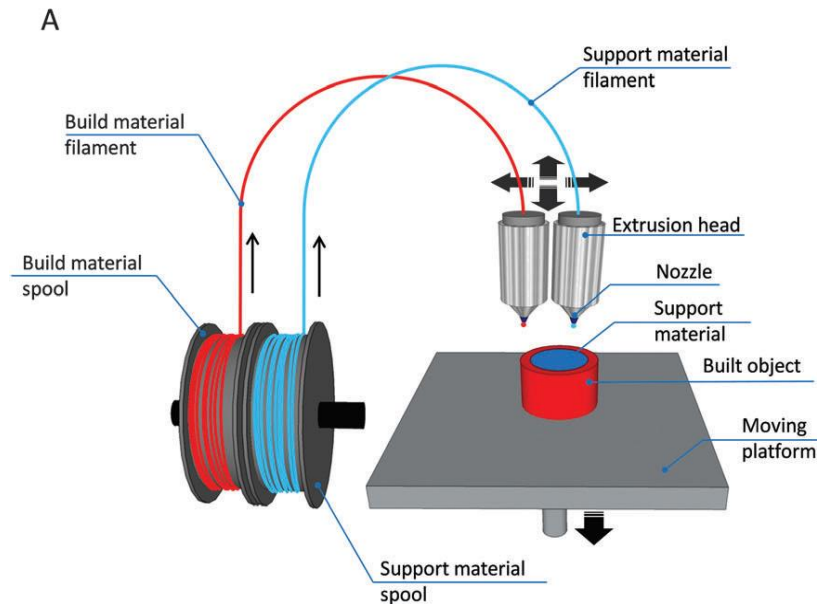


Figure 1-10. Schematic diagram of fused deposition modeling (FDM) [39]

### 1.3.2. Advantages and limitations of AM processes

Advantages are as follows:

- The main advantages of the FDM process are that no resins is required to be cured and there is no need for chemical post-processing, less expensive machine and materials resulting in a more cost-effective process [42].
- Raw material usage and energy consumption are reduced [33].

- Complex designs with several hollow parts can only be obtained by additive manufacturing since these parts are printed together with the solid portions in a layer-by-layer fashion [39].

Limitations are as follows:

- Materials used for rapid prototyping are limited. It is clear that it is not possible to print all commonly used manufacturing materials such as metals and ceramics [43][35].
- In FDM process, the resolution on the z-axis is low compared to other AM process (0.25 mm) requiring a finishing process if a smooth surface is needed and it is a slow process sometimes taking days to build large complex parts [35]
- Size limitation: AM processes are not capable of creating large size parts due to lack of materials strength. Moreover, the amount of time needed for building the large size objects is extended [33].
- Imperfection: AM parts often have a rough and ribbed surface finish. That is because of either the large-sized powder particles or plastic beads [33].

### 1.3.3. Applications

- 1) Lightweight Machines: It is possible to create lightweight parts by AM technology. In the automotive and aerospace industry, the main purpose is to make the lightest structures such as practical car or aircraft while securing safety.

With AM technologies, hollow structures can be made since less material is used [44][35].

2) Architectural Modeling: making architectural modeling is a difficult task for the architectures. AM technology can provide them models very fast without worrying about the complexity of the design [35].

Stereolithography is an appropriate process for the architectural modeling due to the printing resolution [45][46][47][48].

3) Medical Applications: AM technologies have a wide range of applications in the medical world. Dentists have used AM technology to build a plaster model of a patient mouth with a process like stereolithography, selective laser sintering and electron beam melting [49][50]. Bone transplants also can be printed by AM methods which makes it possible to have an identical transplant to the original [51]. The mechanical strength of these implants are higher than others produced by other methods [52].

4) Additive Manufacturing in Art: AM technologies are a widespread tool for the artist in the fashion, furniture, and lighting industry. There are companies that produce furnishing complements, lightning, and accessories including clothes using SLS [53].

## 2. Experimental procedures

In this chapter, the experimental procedures of copper electroplating on both planar geometry and additive manufactured parts in three different electroplating modes (galvanostatic, potentiostatic and pulsed potentiostatic plating) are discussed.

The first outline specifies the electroplating process including preparation of substrate and electrolyte, determination of the I-V relationship for electroplating by using rotary disk electrode (RDE), investigation of different plating parameters for three conditions, coating characterization including coatings thickness measurement, coating mass measurement, surface roughness measurement using confocal laser scanning microscopy and morphology characterization using scanning electron microscopy (SEM).

In the second part, the procedure of printing a 3D part by FDM printer, electroless copper plating process for subsequent electroplating will be described.

### 2.1. Substrate preparation

All coatings were deposited on 110-annealed copper (McMaster-Carr) with a rectangle shape of 10 x 15 mm<sup>2</sup> and 0.8 mm thickness at room temperature and atmospheric pressure. First, the substrate surfaces were cleaned with alcohol to eliminate contamination, mainly from oil or grease. The Substrates were polished before each experiment using aluminum oxide (Al<sub>2</sub>O<sub>3</sub>) with the particle size of ~1 μm to get mirror surface finish.

In order to test the reproducibility of the initial surface roughness of the prepared samples, hand polishing of at least three samples have been carried out. The substrate surface roughness (Sa ~ 0.32±0.26 μm) was determined by 3D confocal laser microscope (Olympus OLS4000). It was

found that the surface roughness of the substrates after polishing are approximately the same, confirming the repeatability of the polishing process.

In the final step, the substrates are cleaned by blowing compressed air jets to remove embedded grit residues on the surface as much as possible.

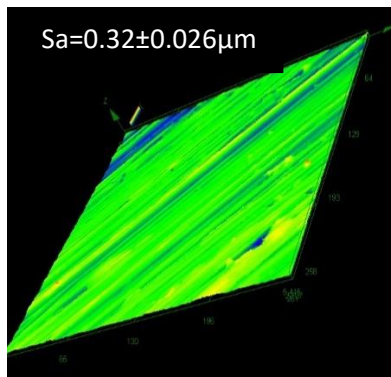


*Figure 2-1. Surface roughness measurement of the copper substrate after preparation obtained by confocal laser microscopy*

## 2.2. Preparation of Copper deposition electrolyte and Electrochemical cell

For the copper electroplating, an electrolytic solution was prepared with deionized water containing 1 M  $\text{H}_2\text{SO}_4$  (98.08%, J.T.Baker) and 0.5 M  $\text{CuSO}_4 \cdot 5 \text{H}_2\text{O}$  (98%, Sigma-Aldrich) that delivers the necessary copper(II)-ions for the deposition (see Figure 2-2).

Prepared electrolyte, 0.5 M  $\text{CuSO}_4 \cdot 5 \text{H}_2\text{O}$ , 1 M  $\text{H}_2\text{SO}_4$ , DI water



*Figure 2-2. Electrolyte preparation*

The working electrode was a rectangle copper plate of 10 x 50 mm<sup>2</sup> and 0.8 mm thickness in which the exposed area is 2 x (10 x 15) mm<sup>2</sup> which was located in the center of the cell.

The counter electrode was a cylindrical copper sheet which surrounds the working electrode to make sure there is always a certain distance between the WE and CE (4 cm).

The reference electrode was a 1 mm diameter copper wire located in the separate compartment of the cell near the working electrode (see Figure 2-3).



*Figure 2-3. Electrochemical cell*

The electrochemical cell contains three electrodes which are connected to the potentiostat/galvanostat (EC19, SRS) capable of keeping the potential/current through an electrolytic cell constant (see Figure 2-4).

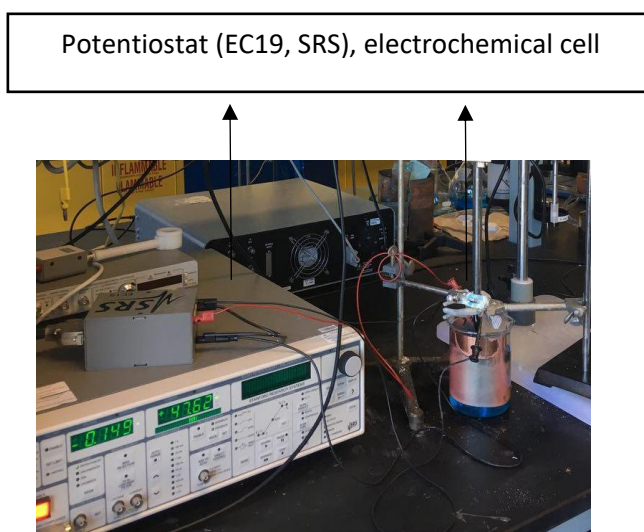


*Figure 2-4. Experimental system*

### 2.3. Polarization curve using a rotary disk electrode (RDE) and in-house developed ECTK software

Rotary disk electrode (RDE) is a hydrodynamic working electrode rotating in the electrolyte. A copper disk of 4 mm diameter embedded in an inert non-conductive polymer connected to an electric motor to be able to fine control of the electrode's rotating rate was used.

The counter and reference electrodes are a copper strip and a copper wire, respectively. The RDE is connected to the potentiostat which is driven by an in-house developed software (EC301, ECTK, Ref: <https://sourceforge.net/projects/ectk/>).

The current-potential relationship (polarization curve) is recorded while the copper disk (surface area:  $0.5 \text{ cm}^2$ ) electrode is rotating in a solution containing  $0.15 \text{ M CuSO}_4$  and  $0.5 \text{ M H}_2\text{SO}_4$ , over a potential range from 0 to  $-800 \text{ mV}$  with an angular velocity of 100, 300 and 1000 rpm and scan rate of  $0.001 \text{ V/S}$  (quasi-static process) to see the effect of angular velocity on limiting current density.

Polarization curve of the prepared copper sample (surface area:  $3 \text{ cm}^2$ ) in the solution containing  $0.5 \text{ M CuSO}_4$  and  $1 \text{ M H}_2\text{SO}_4$  is obtained while the potential range is between 0 to  $-800 \text{ mV}$  with zero angular velocity and scan rate of  $0.001 \text{ V/S}$ .

Figure 2-5 shows the RDE compartments and ECTK script used for obtaining polarization curve of the prepared copper substrate with surface area of  $3 \text{ cm}^2$  with angular velocity of zero.

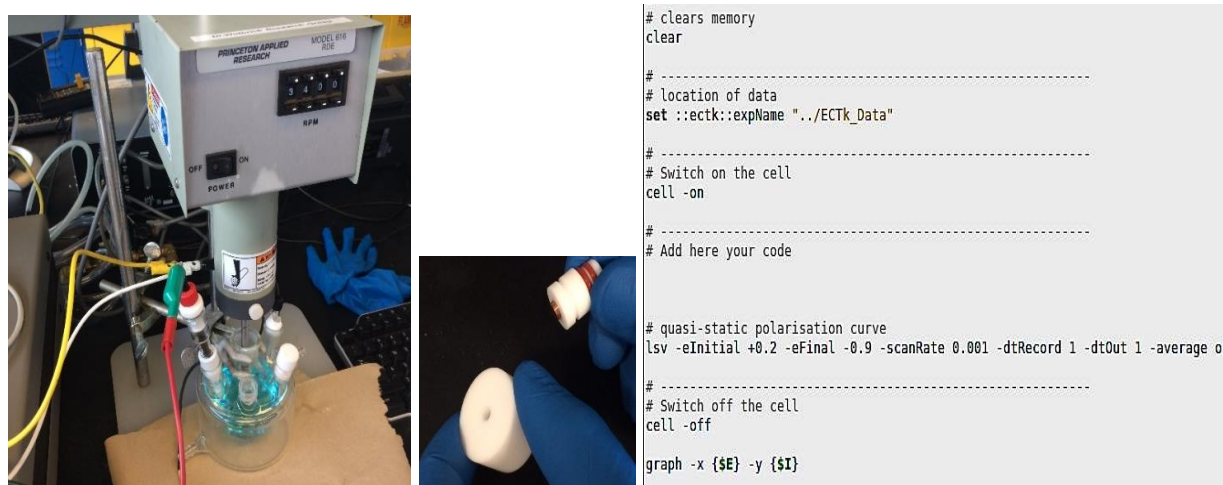


*Figure 2-5. Rotary disk electrode compartments assembling and ECTK script*

## 2.4. Electroplating process

Electroplating process has been carried out in the prepared electrolyte in three different modes; potentiostatic (by applying constant potential), galvanostatic (by applying constant cathodic current) and pulse potentiostatic mode (by applying anodic and cathodic potentials).

The potentiostat (see Figure 2-6) is driven by the in-house developed software (ECTK) capable of controlling the charge at which the experiment will stop once the desired charge is provided.

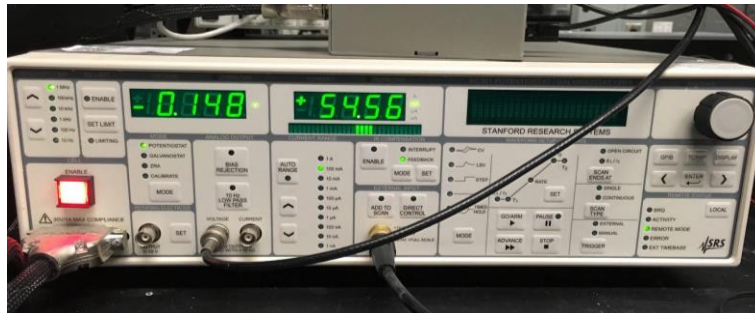


*Figure 2-6. Potentiostat/Galvanostat*

### 2.4.1. Galvanostatic mode

In the galvanostatic mode, prepared copper samples are electroplated at a variety of current densities (5, 10, 15 mA/cm<sup>2</sup>) while keeping the electric charge constant (0.33 C/mm<sup>2</sup>). 5 mA/cm<sup>2</sup> is chosen to determine the effect of electric charge on thickness, surface roughness and morphology of the coatings.

## 2.4.2. Potentiostatic mode

In potentiostatic mode, prepared copper plates are electroplated at a variety of potentials (-150, -200, -350, -400, -500, -750 and -825mV) while keeping the electric charge constant (0.13 C/mm<sup>2</sup>). Subsequently, -150 mV potential is chosen to determine the effect of electric charge on thickness, surface roughness and morphology of the coatings.

## 2.4.3. Pulse potentiostatic mode

In the pulse potentiostatic mode, -150 mV is used as the cathodic potential and +100 mV as the anodic potential. The associated electric charges are 0.013 C/mm<sup>2</sup> for the cathodic pulse and 0.0013 C/mm<sup>2</sup> for the anodic pulse ( $Q_{\text{anodic}}=10\% \times Q_{\text{cathodic}}$ ). The experiments are carried out for different total charges at room temperature (23°C) and atmospheric pressure. The total charge can be calculated according to the following equation where the cathodic charge is measured negatively and the anodic charge positively:

$$Q_{\text{total}} = \text{Number of cycles} \times (Q_{\text{cathodic}} + Q_{\text{anodic}}) \quad \text{Eq 2-1}$$

Furthermore, anodic charge of 1% and 30% of the cathodic charge have been also carried out for the specific total charge of 13.8 C/mm<sup>2</sup>. The chosen parameters will be justified later (see section 3.3).

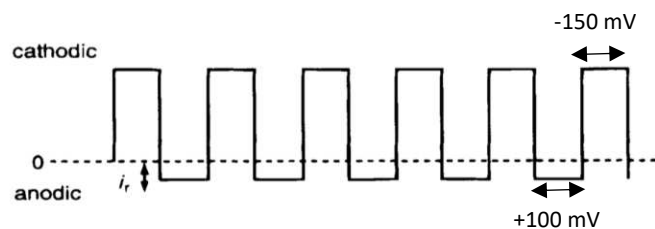


Figure 2-7. Schematic diagram of the pulse potentiostatic electroplating cycles

## 2.5. Coatings characterization

### 2.5.1. Coating thickness and mass measurement

Before and after electroplating, all samples were washed and dried to evaluate the coating thickness distribution along the sample and to measure the mean value of thickness for analysis. The thicknesses were measured by a micrometer (Mitutoyo, resolution of  $\pm 0.01$  mm) randomly at three different points, left, middle and right of samples. (see Figure 2-8). Thickness measurement was carried out for the potentiostatic and galvanostatic deposited samples. However, mass of the samples was measured by a digital scale (OHAUS) for the pulse deposited samples before and after electroplating to have more precise results.



*Figure 2-8. Coating thickness measurement using a micrometer*

### 2.5.2. Coating surface roughness measurement

Confocal laser microscopy has been used to quantify the surface roughness of the coatings and 3D maps of the morphology of the coatings.

### 2.5.3. Scanning Electron Microscopy (SEM)

The coatings were cut into small pieces and washed with ethanol then dried for SEM investigations. They were investigated through a variable pressure scanning electron microscope (SEM, Hitachi, S-3400N). The samples were placed on the carbon film sticking to the conductive sample holder to achieve electrical conduction of the observed surfaces.

The mapping of micro-regions was conducted through a secondary electron (SE) 3D detector at voltage 15 KV, pressure 50 Pa, probe current 40 Amp, and at a focusing distance of 5 to 10 mm, allowing for magnification of up to 5000X used in this study.

## 2.6. 3D printing of an ABS part

A 3D model is designed (mountain part) which is converted to STL format. Slicing process is applied using Cura 3D slicing software to obtain a G-code file containing the information of a series of 2D layers. Finally, the printer starts depositing the material layer by layer according to the G-code file.

### 2.6.1. Surface roughness measurement of an ABS part

Since the additive manufactured part is created layer by layer, the surface roughness is different from a place to another place of a part. Therefore, a specific location of the part is considered to measure the surface roughness by confocal laser microscopy (see Figure 2-9).

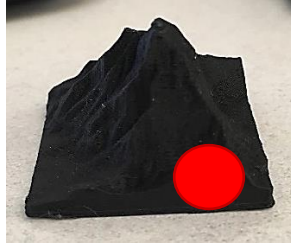


Figure 2-9. The determined location for surface roughness measurement

## 2.7. Copper electroless plating of an ABS printed part

Copper electroless plating has been used to make the exposed surfaces conductive which is followed by electroplating afterward. The process contains five steps: degreasing with oxy-clean, etching, activation, reduction and electroless deposition (see Table 2-1 and Figure 2-10) [54].

Table 2-1. Electroless plating condition for ABS 3D parts

Step	Used Chemicals	Concentration	Time of Immersion (min)	Other Conditions
Degreasing	Oxy-Clean	-	10	Ultrasonic Bath
Etching	Hydrogen Peroxide, Sulphuric Acid	1:5	5	-
Activation	Nickel Acetate	3 g/L	5	Preheat 65C Agitated Solution at 300 rpm
Reduction	Sodium Borohydride	18.9 g/L	5	Agitation with glass stirrer before immersion
Electroless Deposition	CuSO <sub>4</sub> .5H <sub>2</sub> O, NaOH, Disodium Tartrate, Formaldehyde	10 g/L 12 g/L 18 g/L 10ml/L	10	Preheat 38C Agitation During Cycle 100rpm

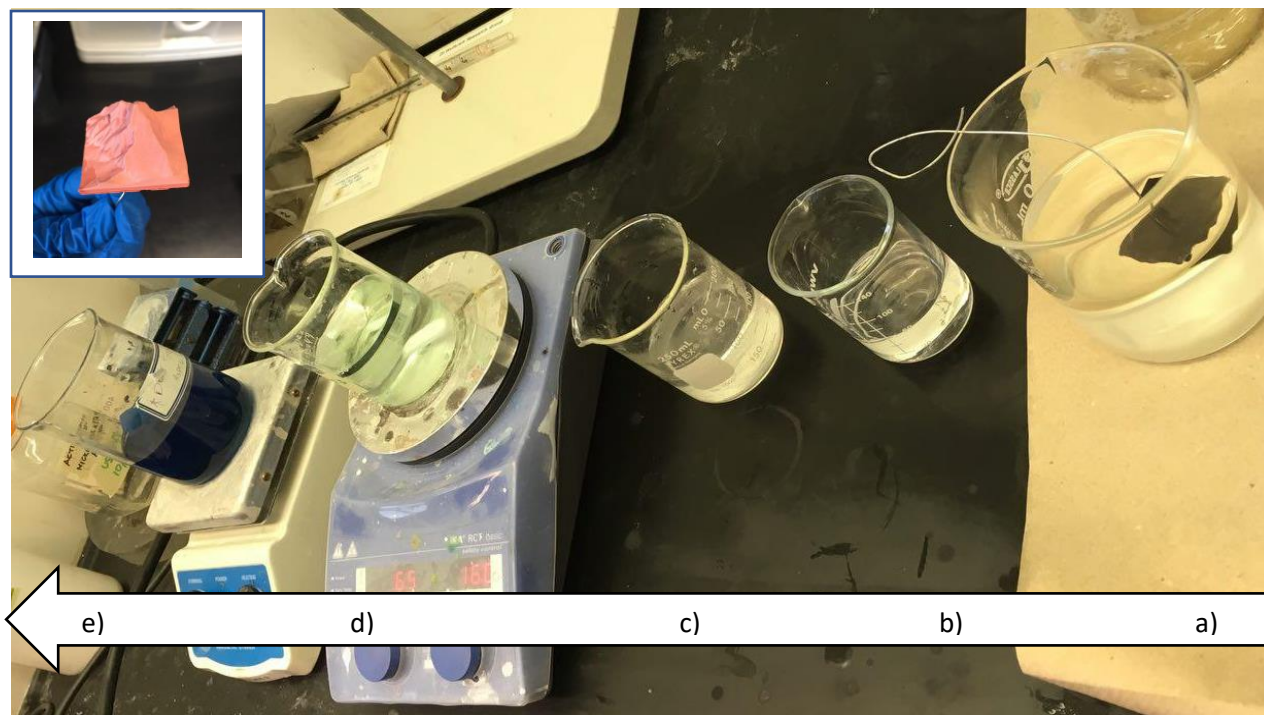


*Figure 2-10. Electroless plating steps; a) Degreasing b) Etching c) Activation d) Reduction e) Electroless deposition*

Dipping in etching solution leads to roughen the surface for good mechanical adhesion, converts the surface from hydrophobic to hydrophilic surface and creates micro pores which acts as bonding sites. Then, sample was activated using Nickel Acetate which was dipped into reduction solution afterward. Black granular material (Nickel Boride) was formed on the surface. In the last step, electroless deposition was carried out.

### 2.7.1. Surface resistance and roughness measurement

The surface resistance and surface roughness of the determined location of the three samples are measured after electroless copper plating by a Multimeter (FLUKE) and confocal laser microscopy, respectively to test the repeatability of the experiment.

High conductivity of the sample is important because if resistance is high, there will be a potential drop over the sample resulting in less uniform thickness of the coating.

## 2.8. Copper electroplating of electroless copper plated ABS part

Electroforming of electroless copper plated ABS part has been done in the same electrolyte for the same depositing charge in three different plating modes according to the optimal parameters obtained from the experiments on the planar geometry samples. For instance, Figure 2-11 shows the electroplating of electroless copper plated ABS part.



*Figure 2-11. Left: ABS printed part, Middle: Electroless copper plated ABS part, Right: Copper electroforming of electroless copper plated part*

### 2.8.1. Surface roughness measurement

The surface roughness of the determined location of three electroformed samples is measured by confocal laser microscopy.

### **3. Results and discussion**

#### **3.1. Potentiostatic plating mode**

In this section, the effect of different parameters on properties of the coatings will be discussed starting from obtaining the polarization curve for deposition electrolyte to get ideas how the system is behaving in different potentials during the cathodic process of copper deposition. Afterwards the studies of the effect of different potentials on properties of the coatings for a same given charge in terms of surface roughness and morphology are performed. After choosing an appropriate potential for the deposition, the effect of charge on surface roughness, thickness, and morphology of the coatings for a same given potential will be represented, specifically.

##### **3.1.1. Polarization curves of two different electrolyte concentrations**

Figure 3-1 compares the obtained polarization curves of the copper disk in an electrolyte containing 0.15 M CuSO<sub>4</sub> and 0.5 M H<sub>2</sub>SO<sub>4</sub> for three different angular velocities (100, 300 and 1000 rpm) [55].

Working electrode, counter and reference electrode used in the experiment were pure copper. The surface area of a working electrode (copper disk) was 0.5 cm<sup>2</sup>.

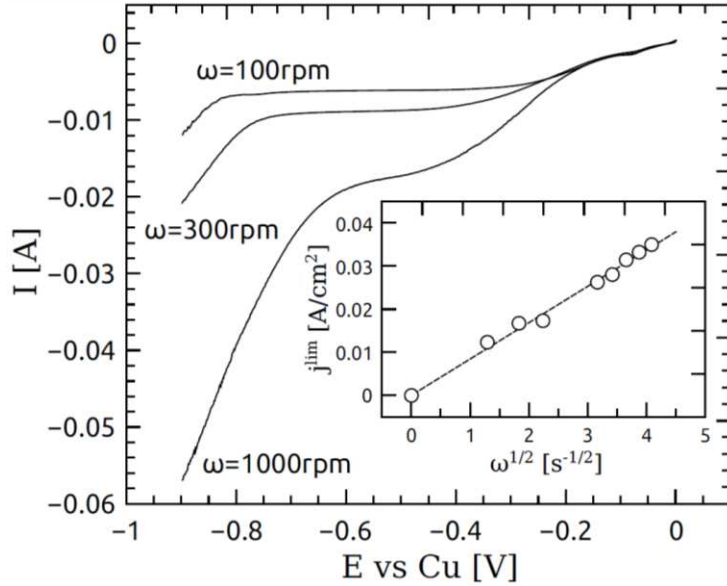
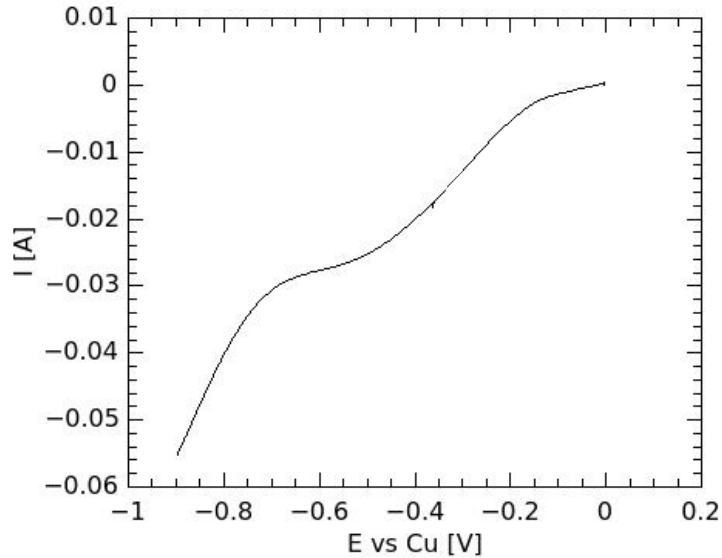


Figure 3-1. Polarization curves for the cathodic process of copper deposition from 0.15 M CuSO<sub>4</sub> in 0.50 M H<sub>2</sub>SO<sub>4</sub> versus Cu at different angular velocities (100, 300 and 1000 rpm)

This polarization curves are consistent with that recently reported in the literature [55]. It can be concluded from Figure 3-1 that the range of potentials belonging to the plateau of the limiting diffusion current density for  $\omega=100$  rpm is approximately between -350 and -750 mV. Furthermore, it is found that by increasing the angular velocity, the limiting current density is increasing (confirming Levich equation:  $j^{\text{lim}} \approx \omega^{1/2}$ ).

Figure 3-2 shows a polarization curve for the copper substrate in an electrolyte containing 0.5 M CuSO<sub>4</sub> and 1M H<sub>2</sub>SO<sub>4</sub> with a scan rate of 0.001 V/S and  $\omega=0$ . The surface area of the working electrode is 3 cm<sup>2</sup>.



*Figure 3-2. Polarization curve for the cathodic process of copper deposition from 0.5 M  $\text{CuSO}_4$  in 1 M  $\text{H}_2\text{SO}_4$*

It can be seen that at higher overpotentials (more cathodic), the hydrogen evolution occurs leading to the remarkable increase in current.

At the values of limiting current density, the species are reduced as they reach the electrode surface.

### 3.1.2. The effect of different potentials on surface roughness of the deposits at an identical charge of $0.13 \text{ C/mm}^2$

According to the polarization curve of the copper deposition electrolyte (0.5 M  $\text{CuSO}_4$  and 1 M  $\text{H}_2\text{SO}_4$ ), seven different potentials: before, within and after the mass transport limited region (-150, -200, -350, -400, -500, -750 and -825 mV) have been applied while keeping the charge

constant at 40 C for a surface area of 300 mm<sup>2</sup> (0.13 C/mm<sup>2</sup>). Note that for high overpotentials (-750 mV and -825 mV) hydrogen evolution takes place.

Figure 3-3 shows the effect of varying potentials on the color of the deposits. As the potential increases from right to left (-150 mV to -825 mV), darker coatings with lower adherence to the substrate and more porous deposits were obtained.

The reason is that the higher the voltage, the more electrons will flow, and the more metal will plate out. However, if the applied voltage is too low, then no current will flow. Moreover, if the voltage is too high, the electrons at the cathode cannot wait for the metal ions to get there and will instead start pulling hydrogen out of the water, depositing hydrogen gas on the cathode. The formation of hydrogen gas and the metal atoms cause the so-called “burning effect” to the depositions.

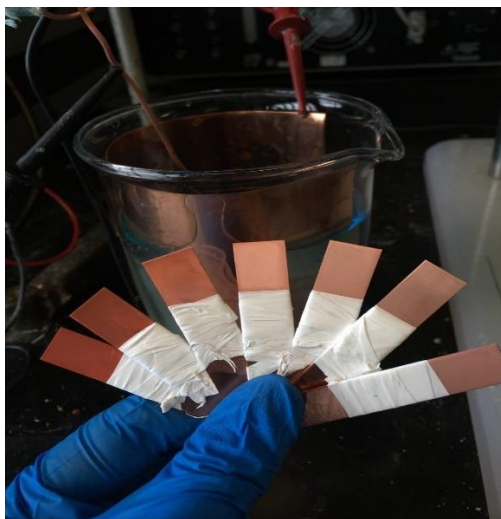


*Figure 3-3. The effect of varying potential on the deposits color for the constant given charge (the applied potential from right to left is -150, -200, -350, -400, -500, -750 and -825 mV)*

Figure 3-4 shows the 3D maps of the morphology of the coatings. As it can be seen, the surface roughness of the deposits is increasing as the potential is increasing due to the higher activation

potential for initiation of nucleation (copper grain size decreases) [55]. Moreover, very porous and disperse copper deposits are obtained at higher overpotentials due to the hydrogen evolution.

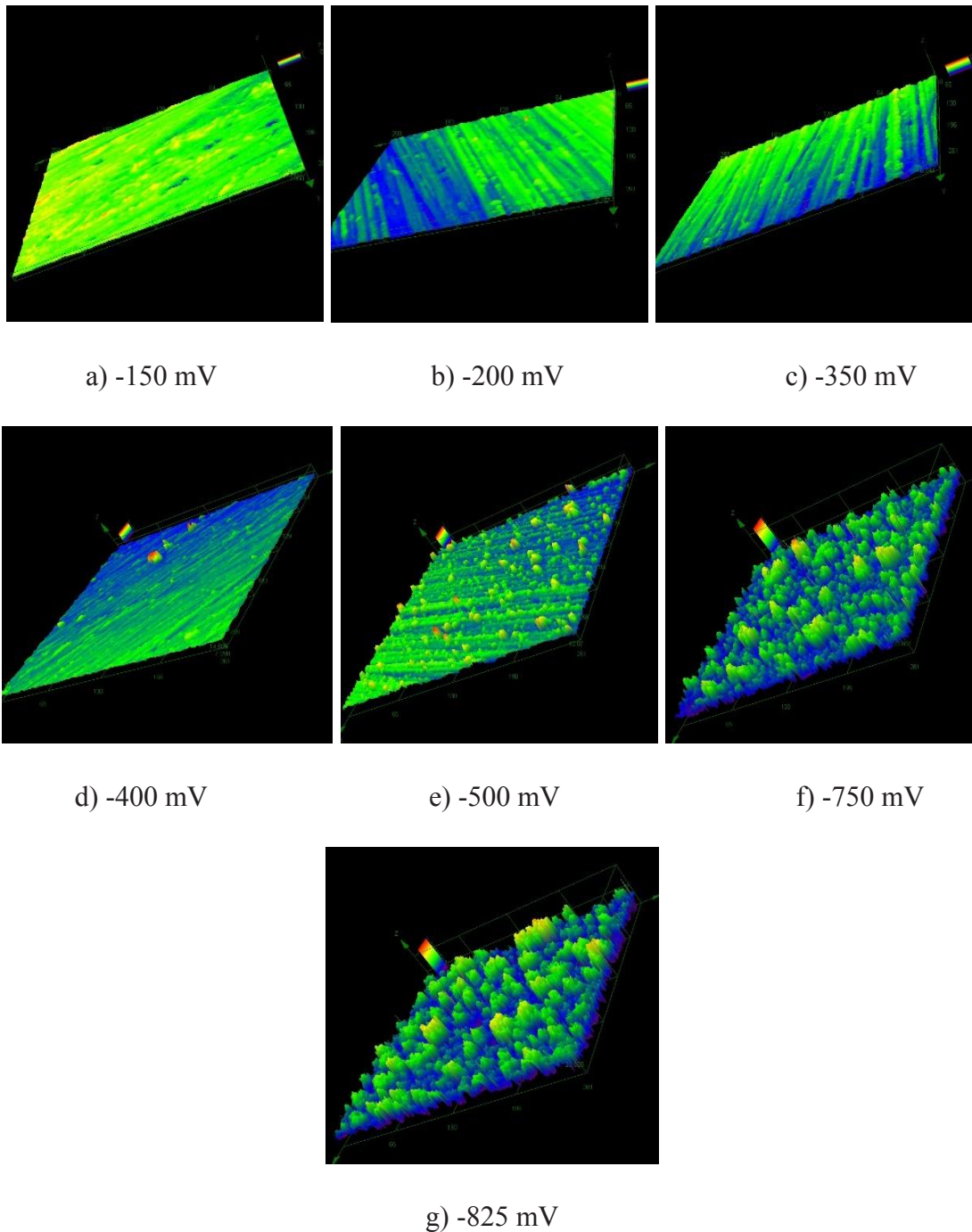


*Figure 3-4. 3D maps of the morphology of the coatings obtained by confocal laser microscopy: a) -150 mV, b) -200 mV, c) -350 mV, d) -400 mV, e) -500 mV, f) -750 mV, g) -825 mV*

Figure 3-5 depicts the surface roughness of the deposits in function of potentials showing that by increasing the potential, the surface roughness is increasing, significantly. This is consistent with the above discussion explaining the change of the color of the deposits.

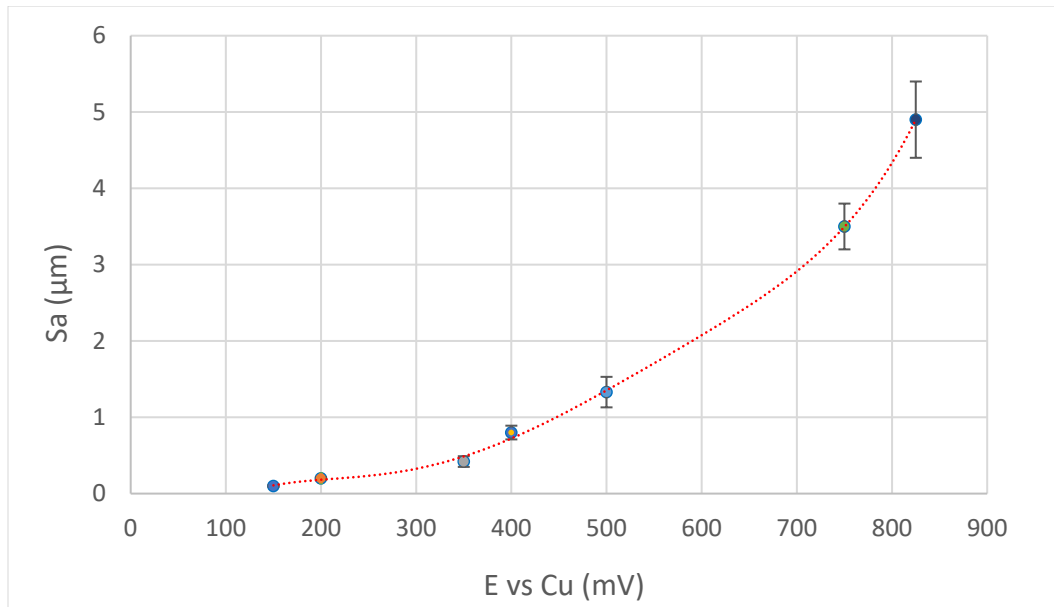
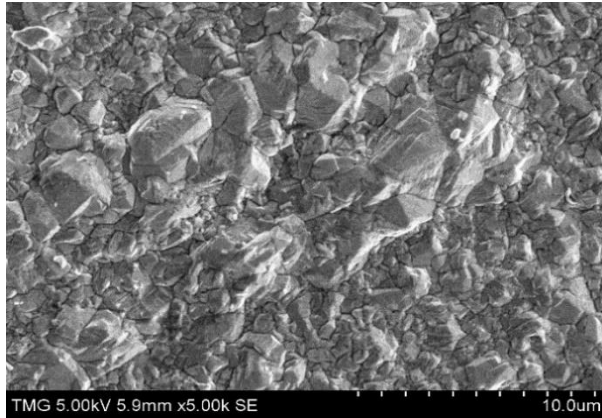


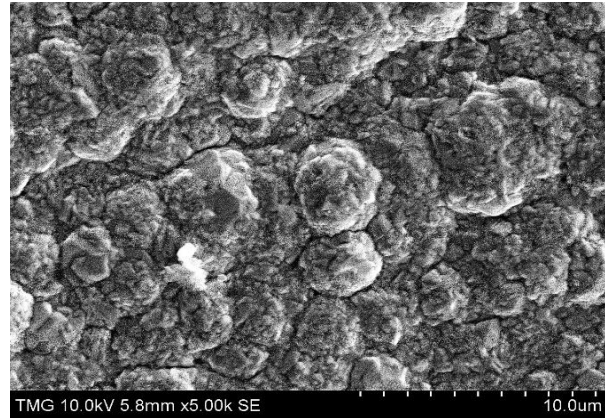
*Figure 3-5. The effect of different potentials on the surface roughness of the deposits at an identical charge of  $0.13 \text{ C/mm}^2$*

### 3.1.3. The effect of different potentials on coatings morphology at an identical charge of $0.13 \text{ C/mm}^2$

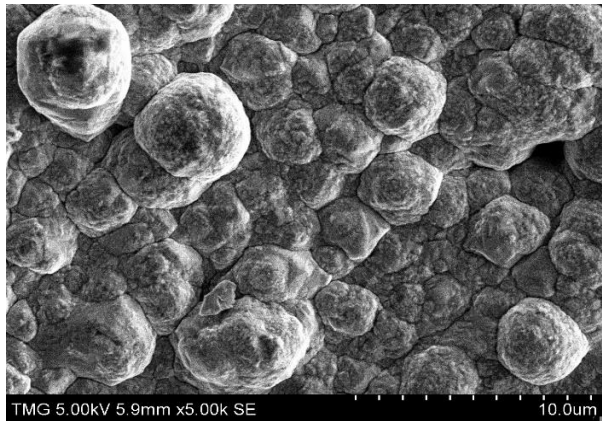
To obtain a better understanding at microscale, SEM investigations of the coatings are performed. Figure 3-6 shows the SEM micrographs of the coatings obtained at potentials of -150mV, -350mV, -400mV, -750mV, and -825mV.



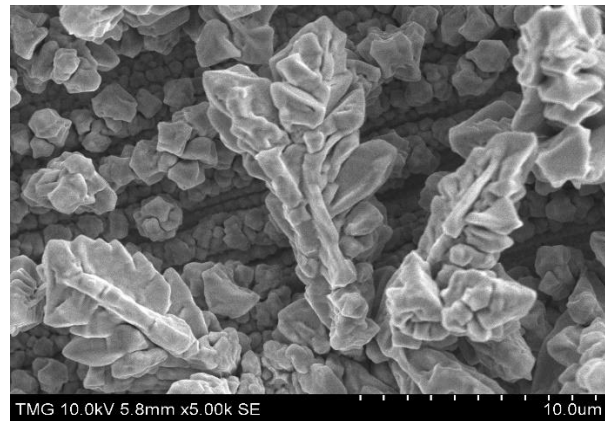
a) -150 mV



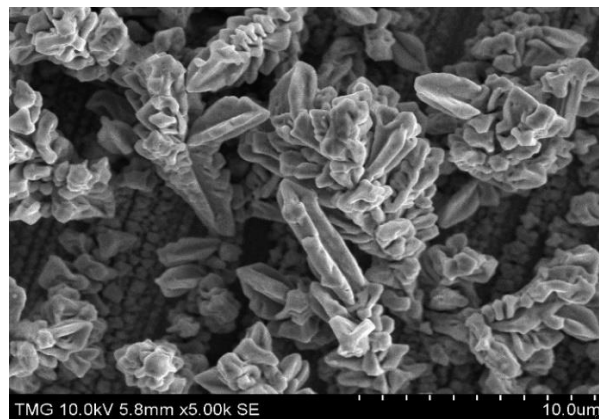
b) -350 mV



c) -400 mV



d) -750 mV



e) -825 mV

*Figure 3-6. Copper deposits obtained at potentials of a) -150mV b) -350mV c) -400mV d) -750mV e) -825 mV. Magnification: X5000, quantity of electricity: 0.13 C/mm<sup>2</sup>*

It can be seen from Figure 3-6 that the increase of the potential from -150 to -400mV, led to the formation of a cauliflower structure which starts to form at the potential of -350mV and can be obviously seen at the potential of -400mV.

It is noticed that by increasing the potential, the size of the copper grain decreases. The increase of the dispersity of copper deposits with increasing deposition overpotentials is primarily due to the increase of the nucleation rate. At these overpotentials, there is no hydrogen co-deposition [56].

At a potential of -725mV, the most important difference is in the shape and size of growing grains, being less globular and smaller in electrodeposition.

Copper deposits obtained at the potential of -725mV presented a mixture of globular-like and dendritic forms.

Disperse and porous structure of the deposit obtained at the overpotential of -825 mV can be obviously seen. The shape and size of copper grains between pores that are caused by the effect of the evolved hydrogen lead to the dendritic morphology at the potential of -825 mV [55].

The structures of these dendrites consist of agglomeration of individual copper grains. Irregular branched, or dendritic deposits are obtained, which may be either useful (for example for powder formation), or undesirable (for example in lithium batteries).

It is well known that the induction time of dendrite growth initiation strongly decreases with increasing overpotential of electrodeposition [57].

At -150 mV potential, the deposit is compact and adhere well to the substrate due to the lack of hydrogen evolution and slow nucleation rate.

Consequently, -150mV is chosen as a potential for the subsequent steps.

### 3.1.4. The effect of charge on thickness and surface roughness of the coatings at a potential of -150 mV

The thickness of the deposits in a function of charge at a potential of -150 mV vs. Cu is shown in Figure 3-7.

The expected deposition thickness ( $\Delta t$ ) for a given charge (Q) can be calculated according to Faraday's law as:

$$\Delta t = \frac{\Delta m}{\rho S} = \frac{QA}{2\rho FS} \quad (\text{deposited mass: } \Delta m = \frac{QA}{2F}) \quad \text{Eq 3-1}$$

where A is the atomic weight of copper (63.55 g/mol), F is the Faraday constant (96 485 C/mol), S is the surface area the of the sample (1.5 cm<sup>2</sup>) and  $\rho$  is the copper density (8.96 g/cm<sup>3</sup>).

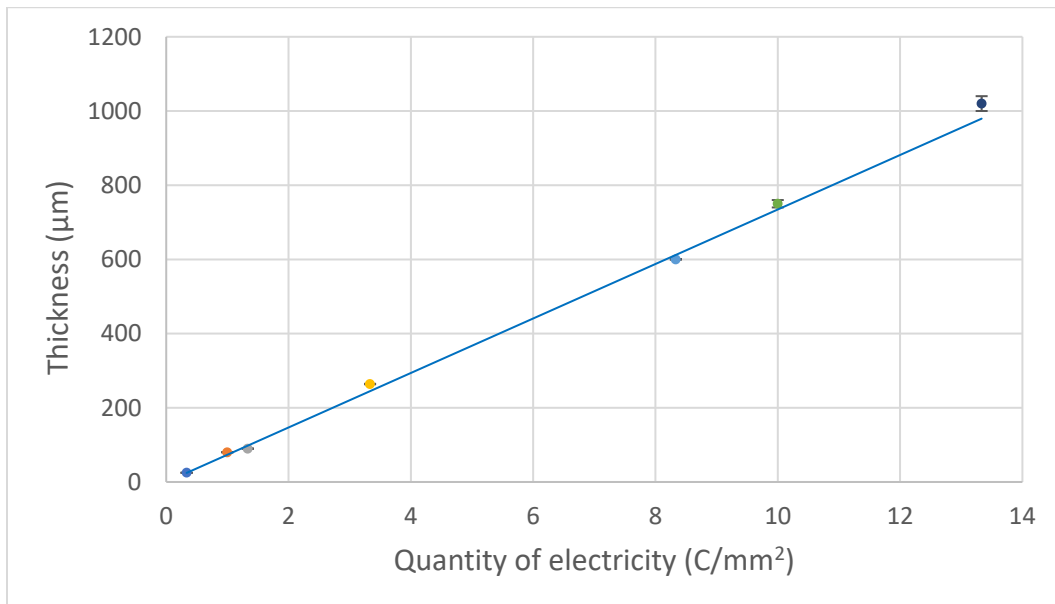
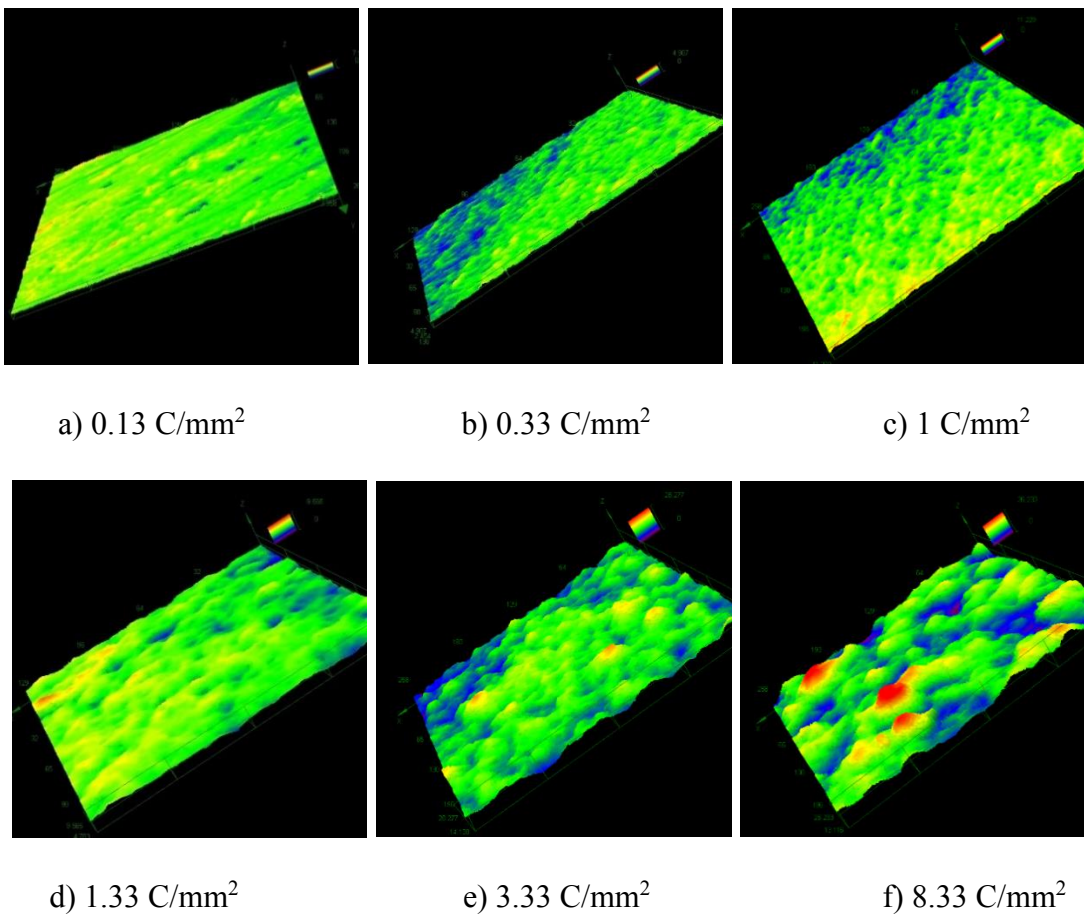
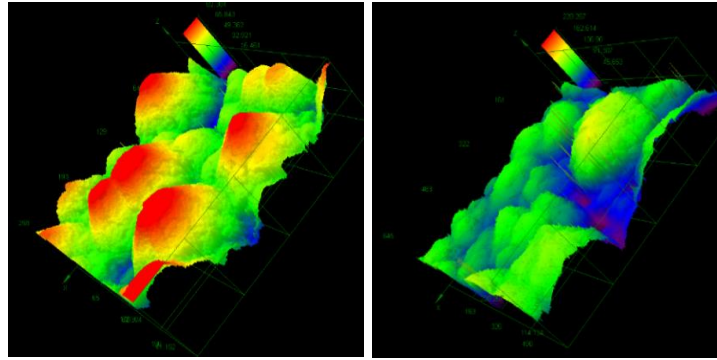


Figure 3-7. The effect of varying total charge on the thickness of the deposits for a given potential of -150mV vs. Cu. Line drawn according to faraday's law (Eq 3-1)

The blue line is drawn according to the Faraday's law equation representing the calculated thickness values, and the dots are the experimentally measured thickness values. A good agreement can be observed. As a result, the thickness can be controlled in potentiostatic plating mode.

Varying the deposition charge affects the surface roughness. Figure 3-8. shows the 3D maps of the morphology of the coatings obtained by confocal laser microscopy for increasing deposition charge.





g) 10 C/mm<sup>2</sup>

h) 13.33 C/mm<sup>2</sup>

Figure 3-8. The 3D maps of the morphology of the coatings obtained by confocal laser microscopy at potential of -150mV for different charges a)0.13C/mm<sup>2</sup> b)0.33C/mm<sup>2</sup> c)1C/mm<sup>2</sup> d)1.33C/mm<sup>2</sup> e)3.33C/mm<sup>2</sup> f)8.33C/mm<sup>2</sup> g)10C/mm<sup>2</sup> h)13.33C/mm<sup>2</sup>

It can be concluded from Figure 3-9 that up to 8.33 C/mm<sup>2</sup>, there is a slight increase in surface roughness which is followed by a remarkable rise from 8.33 C/mm<sup>2</sup> to 13.33 C/mm<sup>2</sup>.

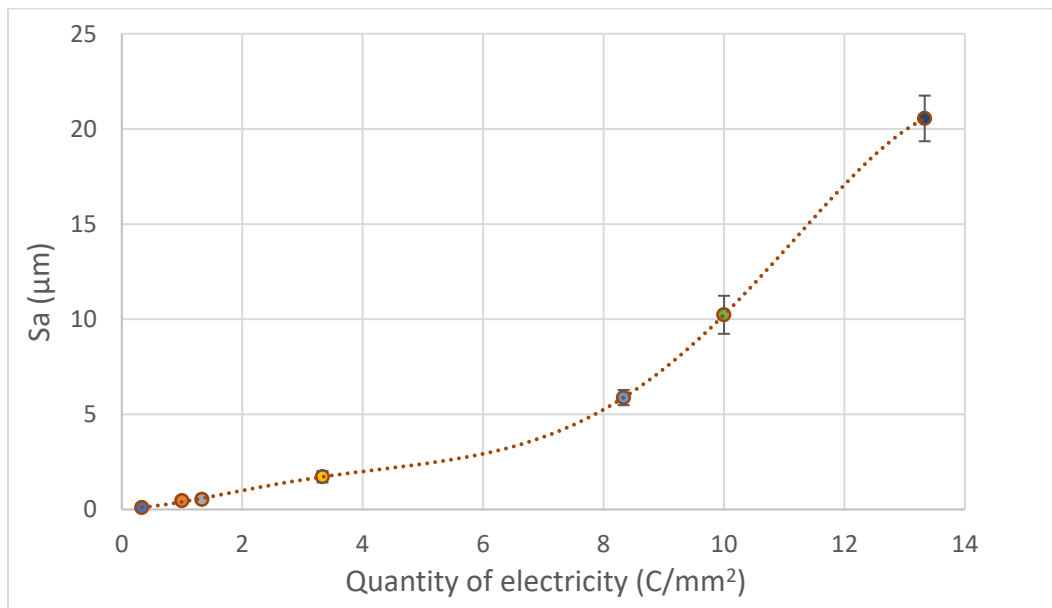
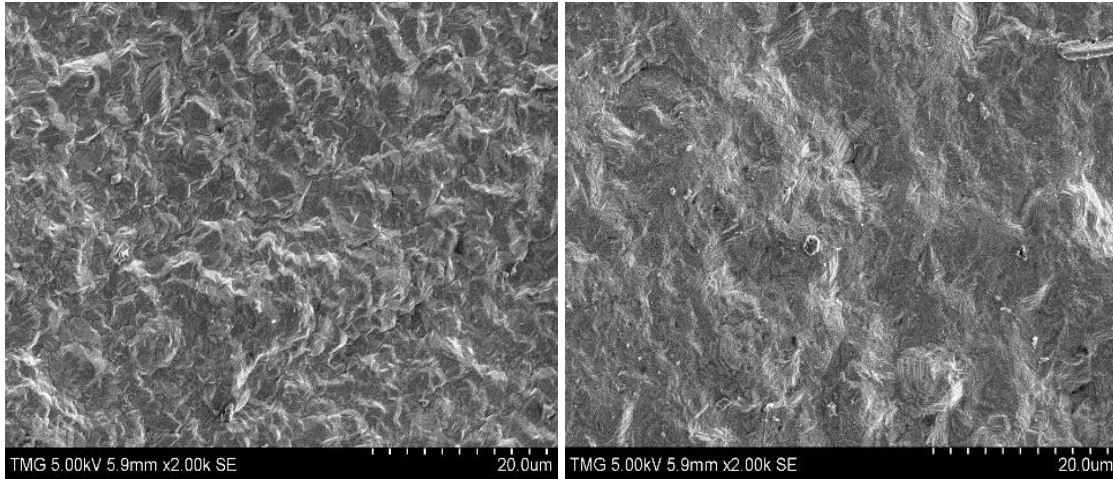


Figure 3-9. The effect of quantity of electricity on surface roughness at a deposition potential of -150 mV

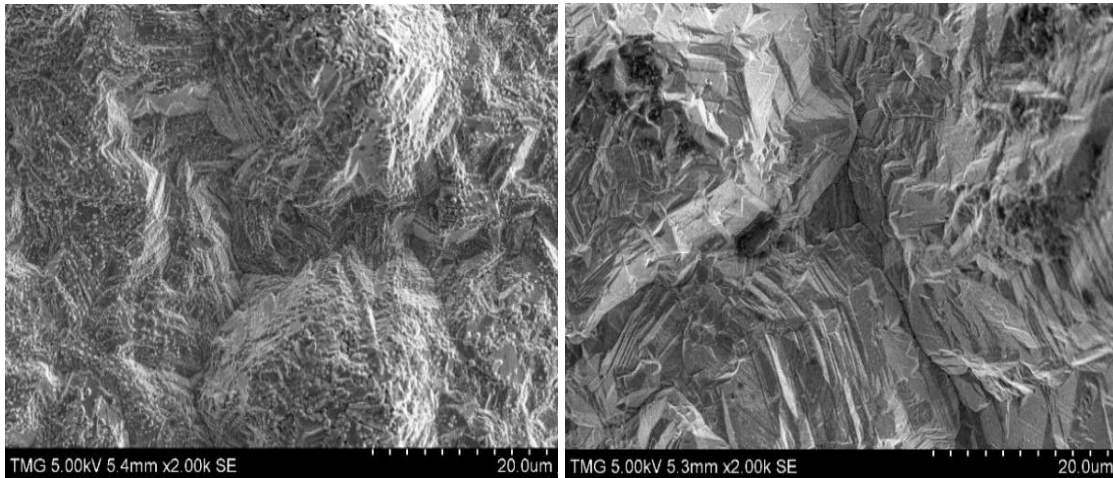
### 3.1.5. The effect of quantity of electricity on coatings morphology at a potential of -150 mV

Figure 3-10 shows the SEM micrographs of the coatings obtained at the different quantity of electricity at a potential of -150mV.



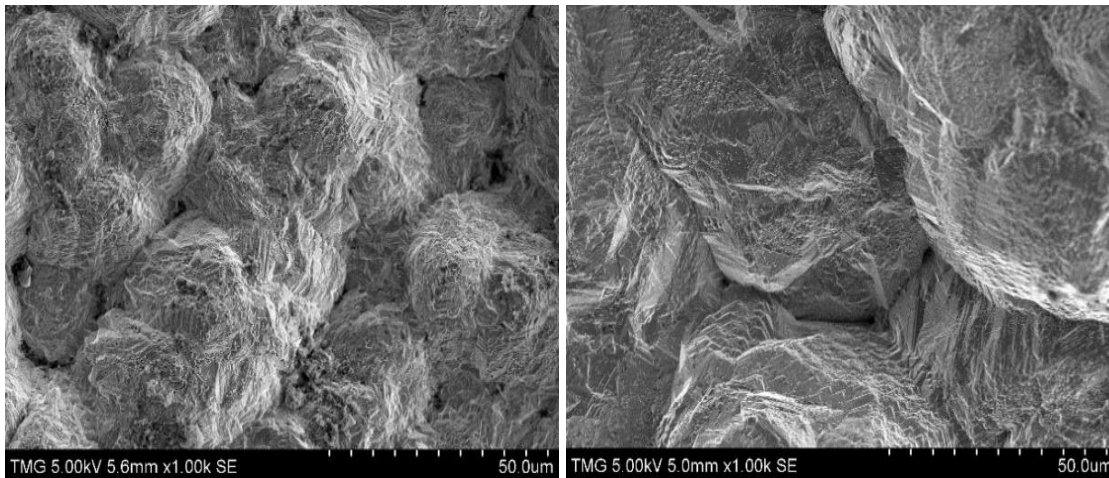
a) 0.33 C/mm<sup>2</sup> X2000

b) 1.33 C/mm<sup>2</sup> X2000



c) 3.33 C/mm<sup>2</sup> X2000

d) 8.33 C/mm<sup>2</sup> X2000



e) 10 C/mm<sup>2</sup> X1000

f) 13.33 C/mm<sup>2</sup> X1000

*Figure 3-10. The SEM micrographs of the coatings obtained at different quantity of electricity at a potential of -150mV. a) 0.33C/mm<sup>2</sup> X2000 b) 1.33 C/mm<sup>2</sup> X2000 c) 3.33 C/mm<sup>2</sup> X2000 d) 8.33C/mm<sup>2</sup> X2000 e) 10C/mm<sup>2</sup> X1000 f) 13.33C/mm<sup>2</sup> X1000*

According to Figure 3-10, enlargement of the grains increases with an increased quantity of electrodeposited metal. These enlarged differences are the consequence of the fact that some smaller grains are consumed by the larger ones (emerging of the grains, grain growth) [56].

In fact, initial small defects serve as preferential nucleation sites for subsequent deposits, increasing progressively the roughness.

It is noted that the word grain does not mean the crystallography grain. It is a commonly used term in this context. Moreover, the reason for the difference in magnification is that at the high quantity of electricity (e and f), grains were not visible at 2000X. Therefore, 1000X was chosen to see the e and f micrographs.

## 3.2. Galvanostatic plating mode

In this part, to find the optimal current density, different current densities were evaluated. After choosing the appropriate current density, the effect of charge on different parameters such as thickness, surface roughness and morphology of the deposits will be presented.

### 3.2.1. The effect of charge on the thickness and surface roughness of the coatings at a current density of 5 mA/cm<sup>2</sup>

According to Figure 3-11, compares the surface roughness of the coatings obtained by different current densities (5, 10, 15 mA/cm<sup>2</sup>) for the constant charge (0.33 mA/cm<sup>2</sup>). Surface roughness is increasing as the current density is increasing. Consequently, 5 mA/cm<sup>2</sup> is chosen for the following experiments.

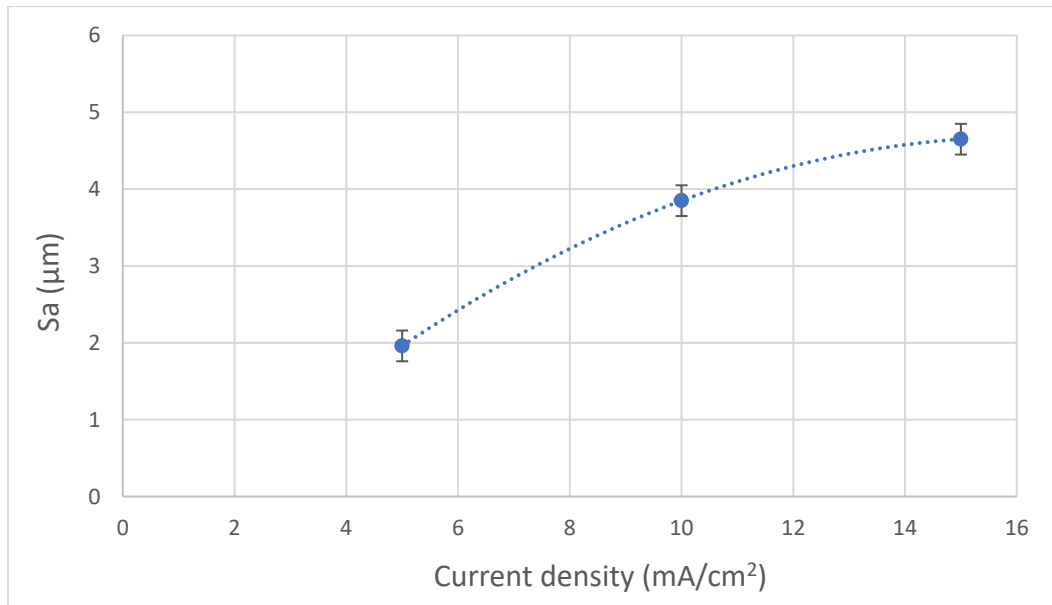


*Figure 3-11. The surface roughness of the coatings in function of current density for a constant charge (0.33 C/mm<sup>2</sup>)*

The thickness of the deposits in a function of charge at a current density of 5 mA/cm<sup>2</sup> is shown in Figure 3-12.

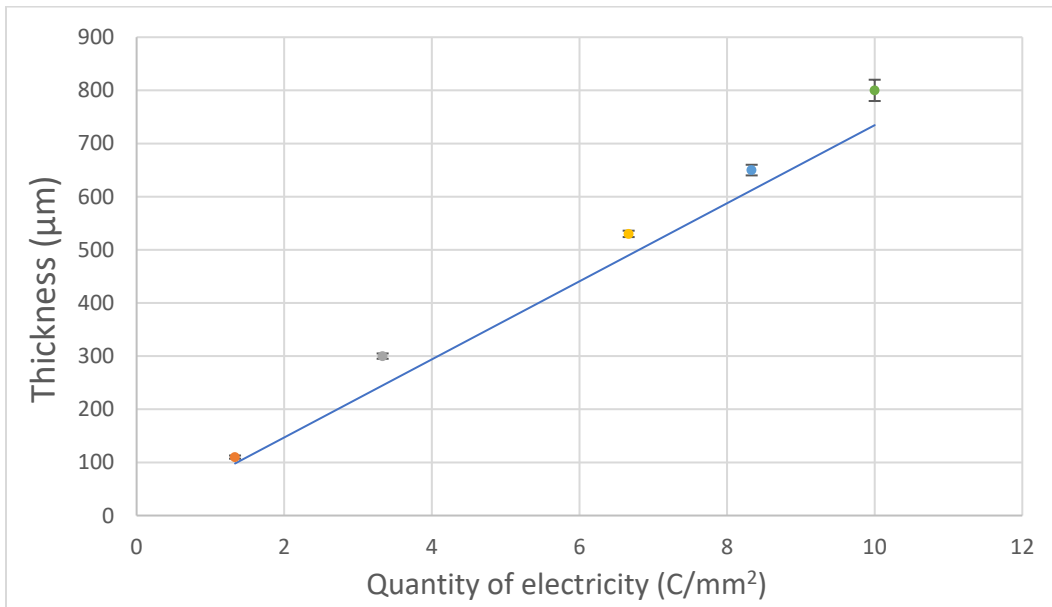
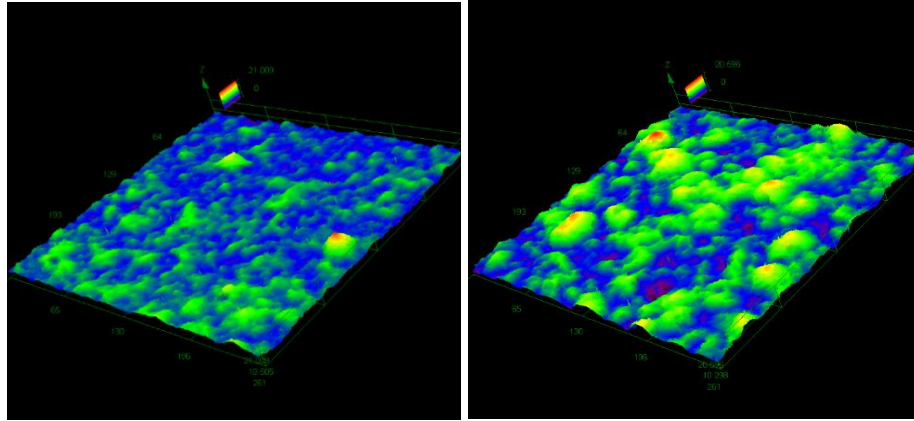


*Figure 3-12. The effect of varying total charge on the thickness of the deposits for a given current density of 5mA/cm<sup>2</sup>*

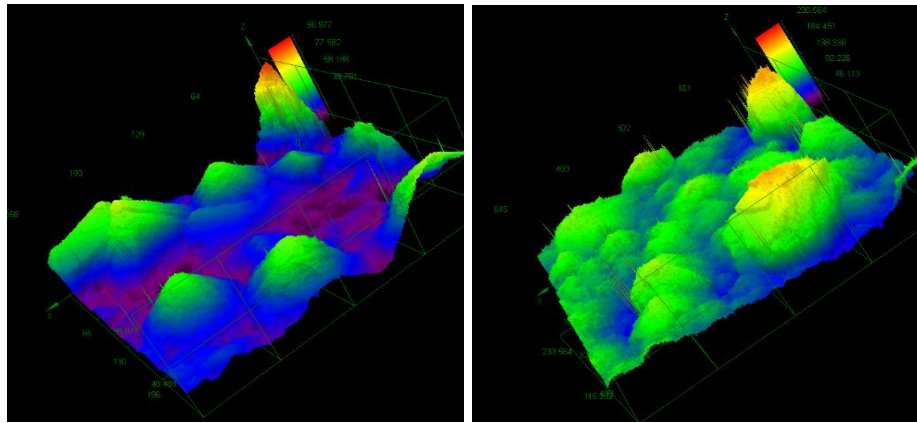
It is obvious from Figure 3-12 that the measured thicknesses are slightly above the calculated thicknesses obtained from Faraday's law (line in the figure). The reason is that the coatings are relatively rough due to the presence of terraces (V-shape sharp edges) as will be seen in SEM micrographs (see Figure 3-15).

Variable charges affect the surface roughness. Figure 3-13 shows the 3D maps of the morphology of the coatings obtained by confocal laser microscopy.



a) 1.33 C/mm<sup>2</sup>

b) 3.33 C/mm<sup>2</sup>



c) 8.33 C/mm<sup>2</sup>

d) 10 C/mm<sup>2</sup>

*Figure 3-13. The 3D maps of the morphology of the coatings obtained by confocal laser microscopy at a current density of 5mA/Cm<sup>2</sup> for different charges a)1.33C/mm<sup>2</sup> b)3.33C/mm<sup>2</sup> c)8.33C/mm<sup>2</sup> d)10C/mm<sup>2</sup>*

It can be concluded from Figure 3-14 that there is a gradual increase in surface roughness of the deposits, reaching to 20  $\mu\text{m}$  at charge 3000 C for the surface area of 300 mm<sup>2</sup> (10 C/mm<sup>2</sup>).

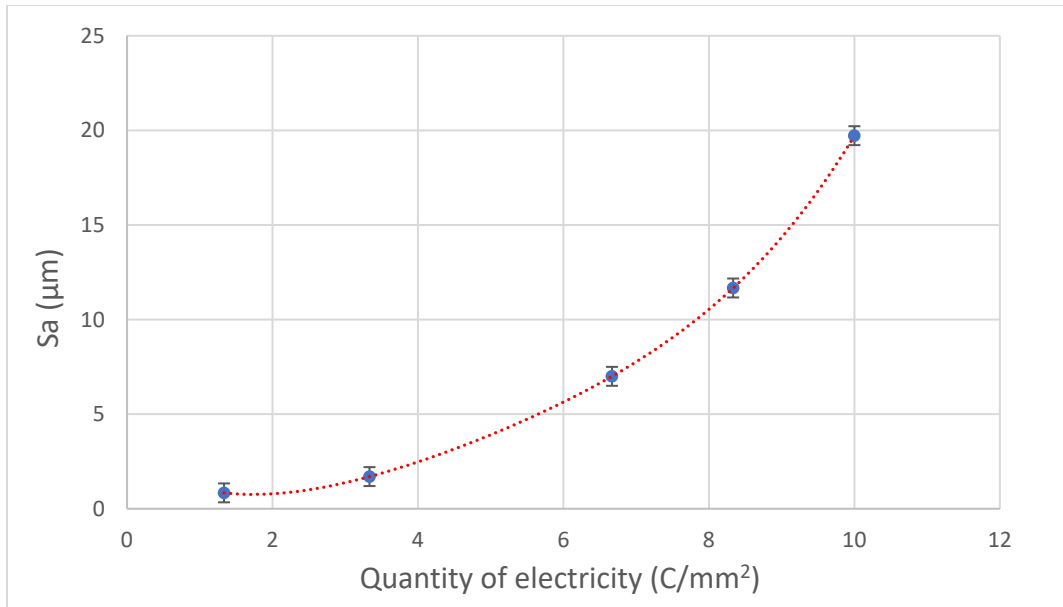
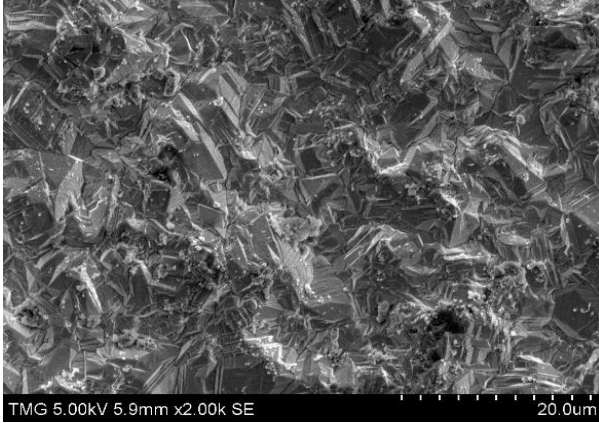


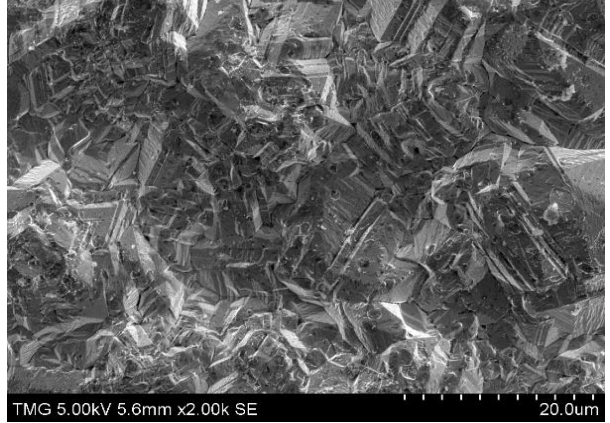
*Figure 3-14. The effect of quantity of electricity on surface roughness at a current density of 5mA/Cm<sup>2</sup>*

### 3.2.2. The effect of quantity of electricity on coatings morphology for a current density of 5 mA/cm<sup>2</sup>

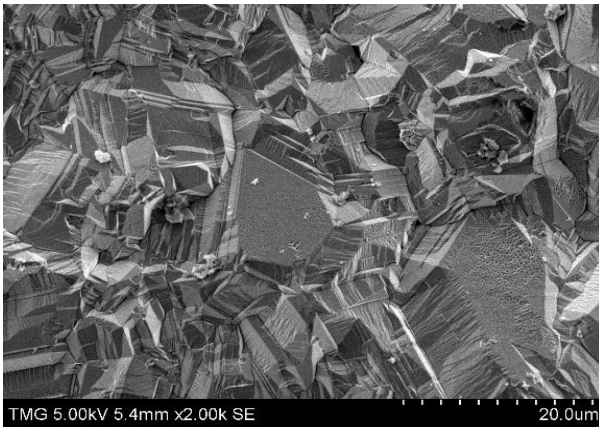
Figure 3-15. shows the SEM micrographs of the coatings obtained at different quantity of electricity at current density of 5 mA/cm<sup>2</sup>.



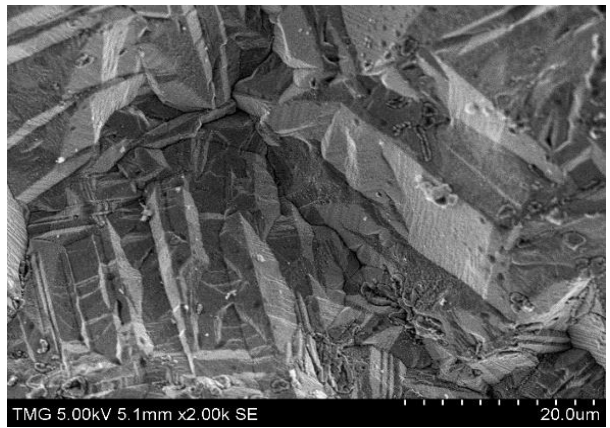
a) 1.33 C/mm<sup>2</sup> X2000



b) 3.33 C/mm<sup>2</sup> X2000



c) 8.33 C/mm<sup>2</sup> X2000



d) 10 C/mm<sup>2</sup> X2000

*Figure 3-15. The SEM micrographs of the coatings obtained at different quantity of electricity at current density of 5mA/Cm<sup>2</sup>. a) 1.33C/mm<sup>2</sup> X2000 b) 3.33C/mm<sup>2</sup> X2000 c) 8.33C/mm<sup>2</sup> X2000 d) 10C/mm<sup>2</sup> X2000*

The character of the morphologies shows the V-shaped grains which start to grow by increasing the quantity of electricity [58][59].

It should be noticed that in galvanostatic condition ( $I = \text{Const}$ ), the potential is variable which means that the electrochemical reaction dynamics changes over deposition time.

For instance, Figure 3-16 is a recorded plot of the over-potential in function of time at a constant current density ( $5 \text{ mA/cm}^2$ ).

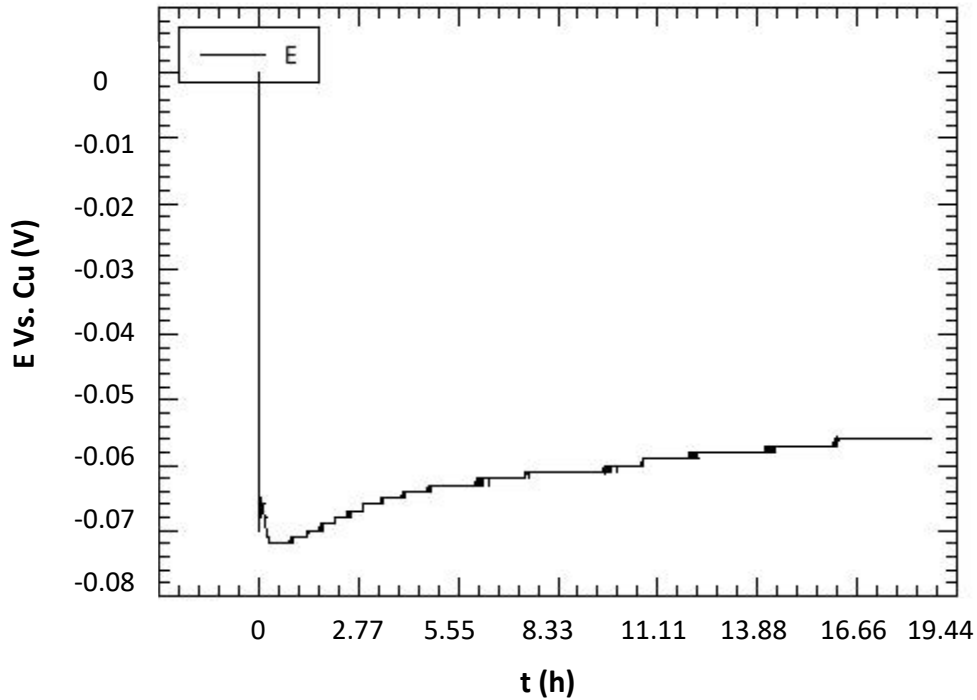


*Figure 3-16. schematic representation of an  $E(t)$  relationship for a constant current density of  $5 \text{ mA/cm}^2$  for a quantity of electricity of  $8.33 \text{ C/mm}^2$*

The initial increase of the potential is due to both the charging of the electric double layer and the establishment of an increasing population of clusters which are followed by decreasing the potential due to the growing of the stable clusters that consume the almost entire current [60].

As it can be seen from the Figure 3-16, the  $E(t)$  relationship curve will never stabilize and varies between  $-70 \text{ mV}$  and  $-50 \text{ mV}$ . This continuous variation is due to the change of surface area as the deposition proceeds (because roughness is increasing).

### 3.3. Pulse-potentiostatic plating mode

As discussed in the literature; a smoother and less porous deposit can be obtained using pulse plating due to the presence of relaxation time or anodic potential during each period. In this section, pulse-reverse plating of copper is evaluated with the goal of improving the surface quality (smoother surface).

First of all, it can be concluded from potentiostatic electroplating that by depositing higher charges, the defects (initial small roughness) grow resulting eventually in a rough surface. In order to decrease the defects and to get a smoother surface, one deposition step which is followed by one polishing step during each period are being carried out leading to the formation of a homogenous surface with more distributed defects. Of course, there are still defects, but they are being more distributed and there are not the same defects that will grow during deposition. That is why thicker deposit can be created while keeping the surface roughness low.

In order to proceed, one-layer deposition which has the thickness higher than the roughness is made to make sure that the surface is fully covered. Afterward polishing is carried out.

According to Figure 3-9, the surface roughness of the deposits obtained at low quantity of electricity (less than  $2 \text{ C/mm}^2$ ) is below  $1 \mu\text{m}$ . Consequently,  $1 \mu\text{m}$  is chosen as the depositing thickness in each period (which corresponding to a charge of  $0.013 \text{ C/mm}^2$ ). Using this method allows putting nice layers on each other to avoid forming the rough surface over the time.

The desired pulses can be achieved by programming in ECTK without using any extra equipment. Required cathodic charge, anodic charge, corresponding potentials and the number of pulses are the input values.

Therefore,  $0.013 \text{ C/mm}^2$  is considered as the cathodic charge which has the corresponding thickness of  $1 \text{ }\mu\text{m}$ , and 10% of the deposition charge is chosen to be the anodic charge. The corresponding potential for the cathodic pulse is  $-150 \text{ mV}$ , and the anodic potential is  $+100 \text{ mV}$ .

Furthermore, the anodic charge of 1% and 30% of cathodic charge is also evaluated for a total quantity of electricity ( $13.8 \text{ C/mm}^2$ ) to compare the obtained thickness and  $S_a$ .

Figure 3-17 shows the pulsating graph contains  $0.013 \text{ C/mm}^2$  cathodic charge and  $0.0013 \text{ C/mm}^2$  anodic charge.

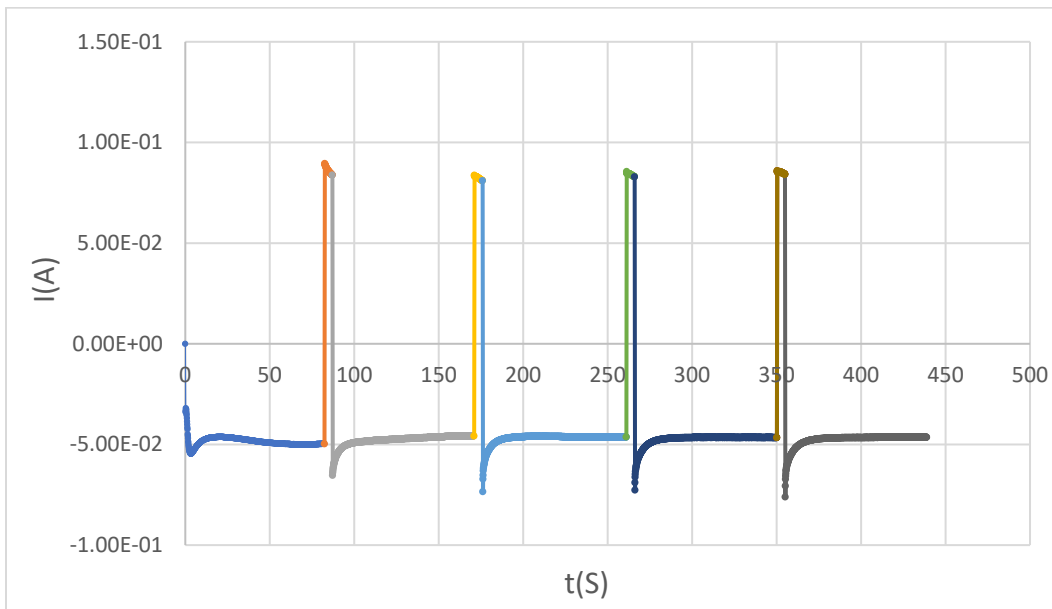
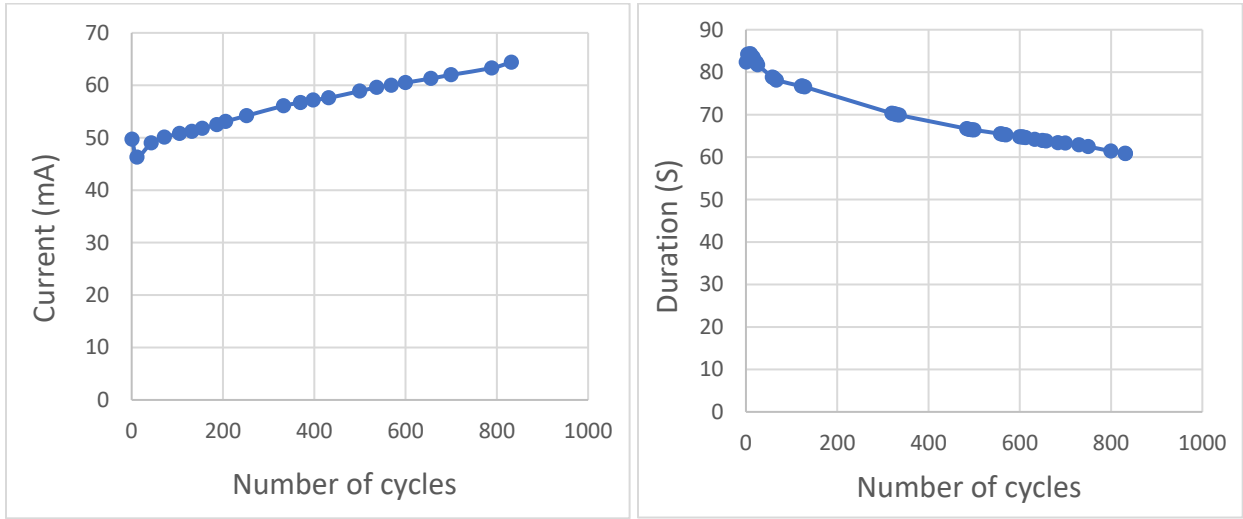


*Figure 3-17. The schematic of I-t of the initial cycles contains  $0.013 \text{ C/mm}^2$  cathodic charge and  $0.0013 \text{ C/mm}^2$  anodic charge (the corresponding potentials are  $-150 \text{ mV}$  and  $+100 \text{ mV}$  vs Cu)*

Figure 3-18 (a) illustrates that by increasing the number of cycles, the cathodic current (deposition current) is increasing gradually. As the deposition continues, the surface area is getting larger and more active surfaces (rougher) form leading to the rise in current (increased roughness).

Figure 3-18 (b) shows the decrease in cathodic pulse duration. According to  $It = Q$ , since the cathodic charge in each cycle is constant, the depositing time decreases while the cathodic current is rising, by increasing the number of cycles.



a)

b)

*Figure 3-18. a) The influence of the number of cycles on the cathodic current for 832 total number of cycles. b) The effect of the number of cycles on the cathodic pulse duration for the 832 total number of cycles*

Like Figure 3-18 (a), Figure 3-19 (a) shows an increase in anodic current (polishing current) as a function of number of cycles. The reason is that by increasing the number of cycles, the surface area is changing due to the increased roughness. According to  $I = j \cdot S$ , where  $I$  (A) is the current,  $j$  (A/m<sup>2</sup>) is the current density and  $S$  (m<sup>2</sup>) is the surface area, by controlling the deposition potential, the anodic current is increasing.

Figure 3-19 (b) shows the decrease in anodic pulse duration. According to  $It = Q$ , since the polishing charge is constant in each anodic pulse, the polishing pulse time decreases while the current is rising, by increasing the number of cycles.

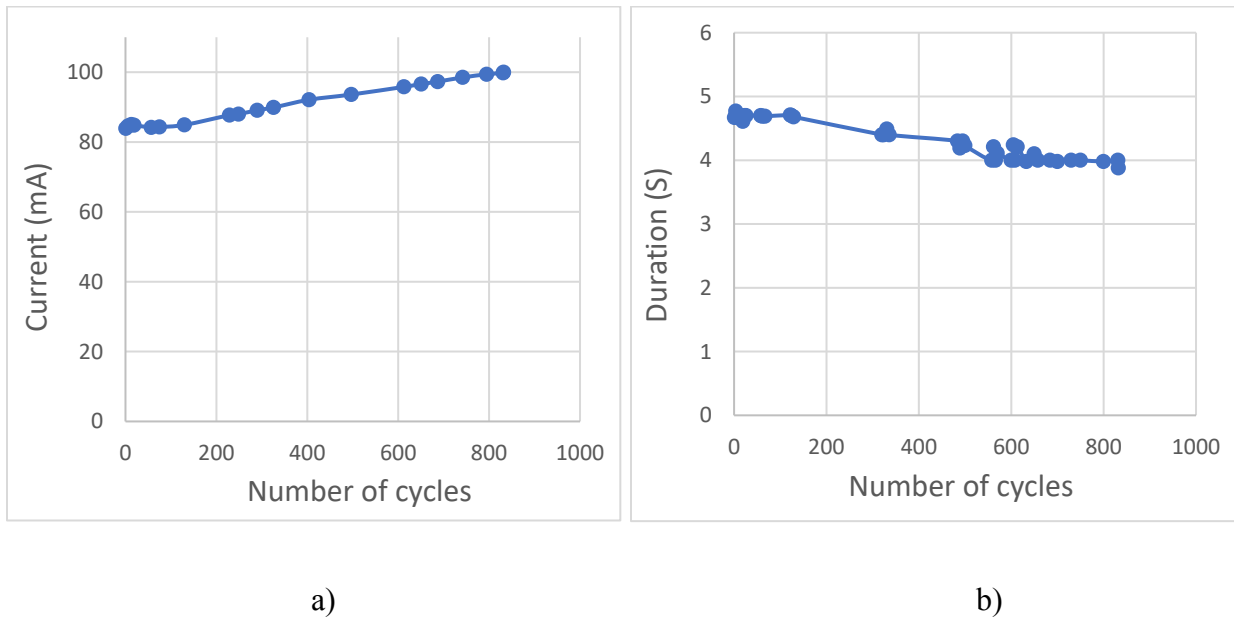
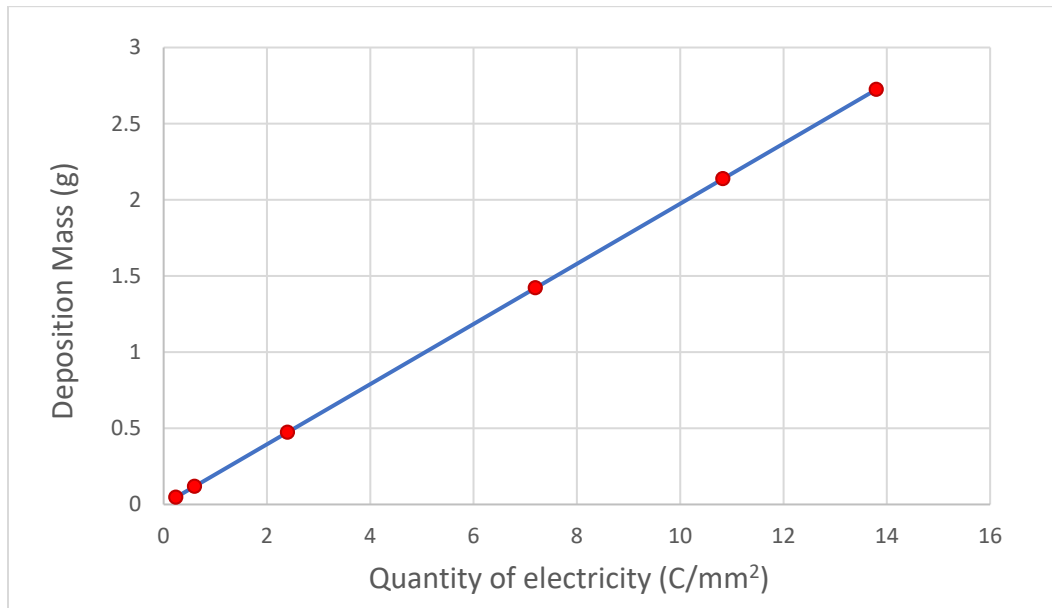


Figure 3-19. a) The influence of the number of cycles on the anodic current for 832 total number of cycles. b) The effect of the number of cycles on the anodic pulse duration for the 832 total number of cycles

### 3.3.1. The effect of total charge on thickness and surface roughness of the coatings obtained by pulse potentiostatic plating

The effect of charge on the mass of 10% polished deposits is shown in Figure 3-20.



*Figure 3-20. The effect of varying total charge on mass of the 10% polished deposits (the cathodic charge: 0.013 C/mm<sup>2</sup>, the anodic charge: 0.0013 C/mm<sup>2</sup>, the cathodic potential: -150 mV, the anodic potential: +100 mV)*

The total quantity of electricity can be obtained by the following equation:

$$Q_{\text{total}} = \text{Number of cycles} * (\text{anodic charge} + \text{cathodic charge})$$

Where the cathodic charge is measured negatively and anodic positively.

The calculated deposited mass of the samples (blue line) are obtained from the Faraday's law

$$(\Delta m = \frac{QA}{2F}).$$

As Figure 3-20 shows, the measured mass of the depositions follows the line showing a good control of the deposition mass in pulse electrodeposition.

Figure 3-21 shows the effect of different anodic charge on the mass of the deposits by keeping the cathodic charge constant at  $0.013 \text{ C/mm}^2$  for the total charge of  $13.8 \text{ C/mm}^2$ .

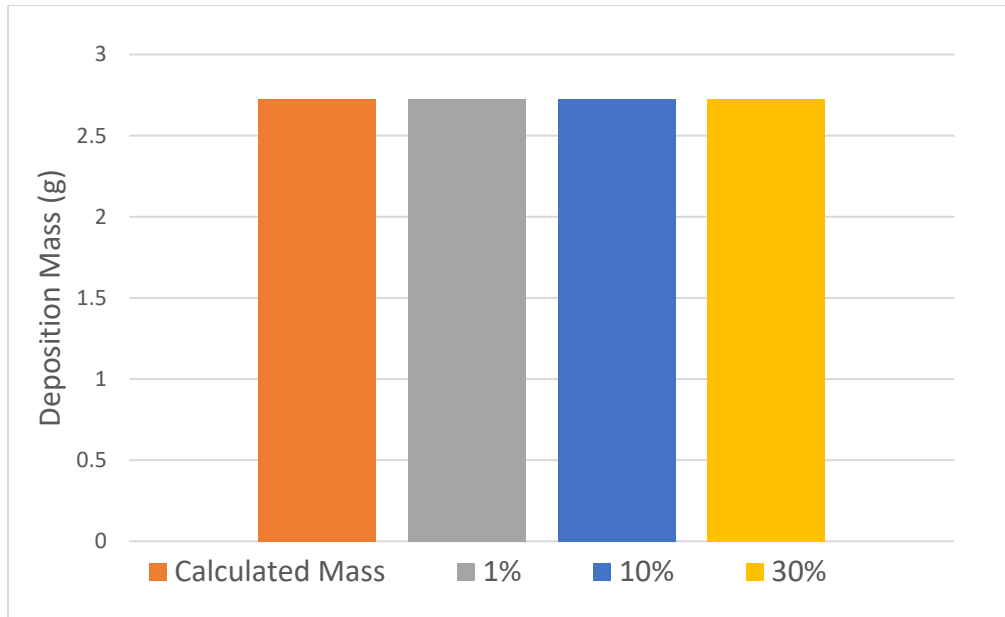


*Figure 3-21. The effect of different anodic charge (1%, 10% and 30% of cathodic charge) on the mass of the deposits by keeping the cathodic charge constant at  $0.013 \text{ C/mm}^2$  for the total charge of  $13.8 \text{ C/mm}^2$*

According to Figure 3-21, the deposition mass for different anodic charges (1%, 10% and 30% of the cathodic charge) is the same as the calculated mass value. The more the polishing charge percentage, the more the number of cycles, because according to  $Q_{\text{total}} = \text{Number of cycles} * (\text{anodic charge} + \text{cathodic charge})$ , by increasing the anodic charge percentage, more material is removed from the deposit, therefore, more cycles are needed to compensate the material loss.

Changing in the total amount of charges affects the surface roughness. Figure 3-22 shows the 3D maps of the morphology of the 10% polished coatings obtained by confocal laser microscopy.

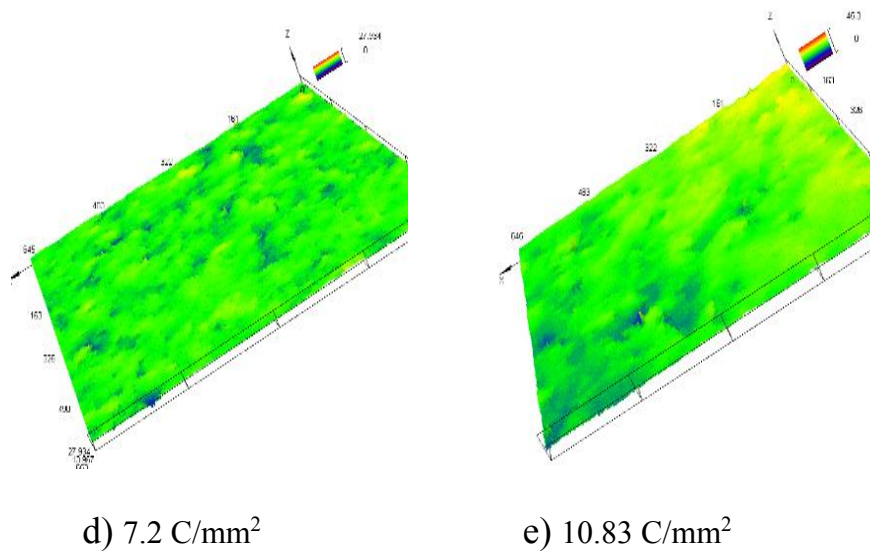
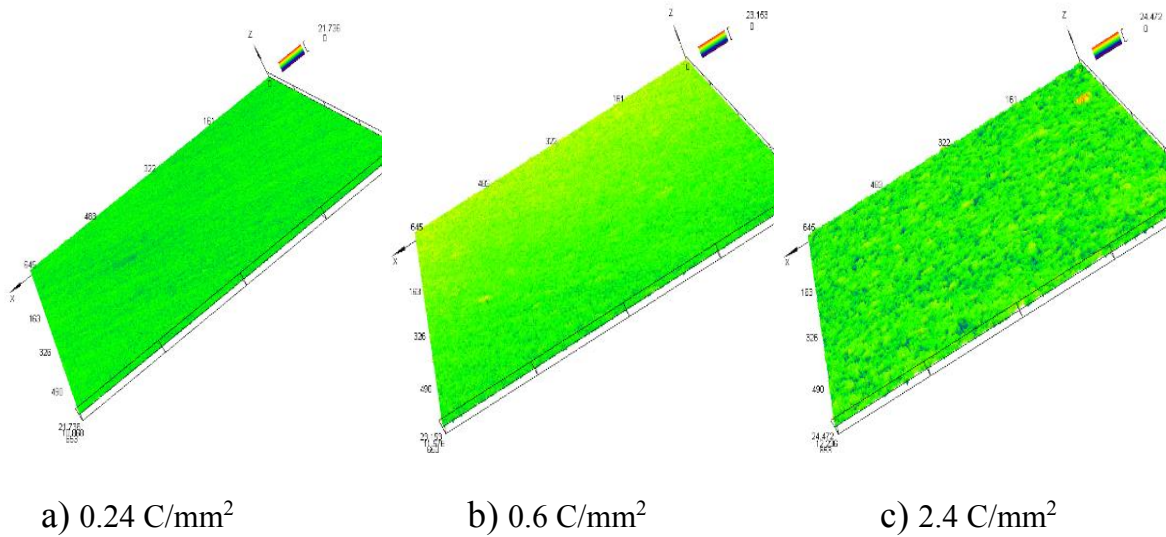


*Figure 3-22. The 3D maps of the morphology of the 10% polished coatings obtained by confocal laser microscopy at certain pulse parameters (4C at -150mV for deposition and 0.4C at +100mV for polishing) for different total charges: a)  $0.24 \text{ C/mm}^2$  b)  $0.6 \text{ C/mm}^2$  c)  $2.4 \text{ C/mm}^2$  d)  $7.2 \text{ C/mm}^2$  e)  $10.83 \text{ C/mm}^2$*

It can be concluded from Figure 3-23 that there is a slight increase in surface roughness of the deposits, reaching to  $4.5 \pm 0.7 \mu\text{m}$  at a charge of 4140 C for a surface area of  $300 \text{ mm}^2$  ( $13.8 \text{ C/mm}^2$ ).

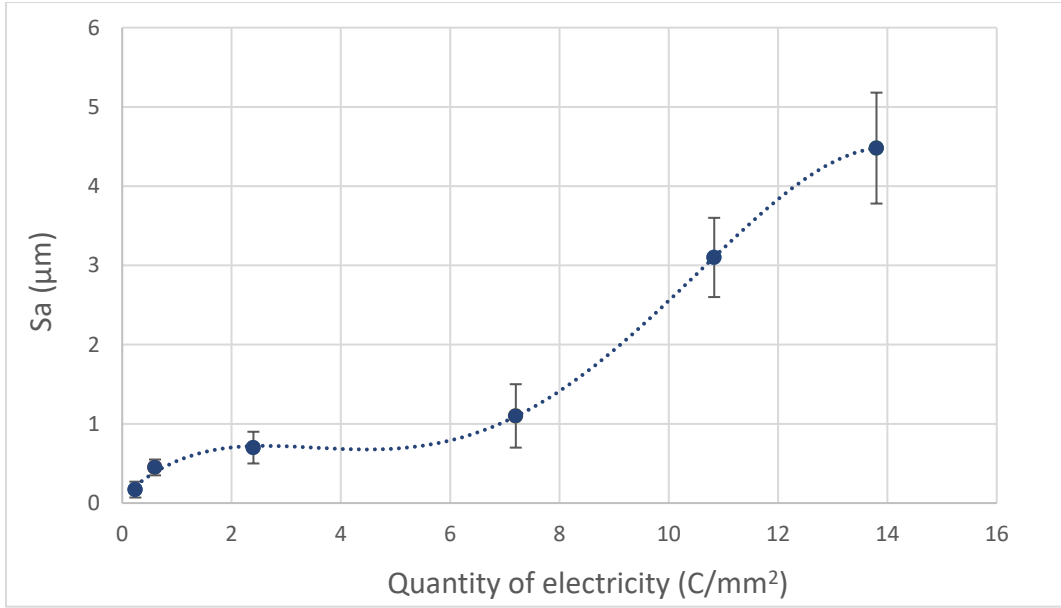


Figure 3-23. The effect of quantity of electricity on surface roughness of the 10% polished deposits. Freely drawn trendline.

Figure 3-24 shows the effect of different anodic charge on the surface roughness of the coatings for the total charge of 13.8 C/mm<sup>2</sup>.

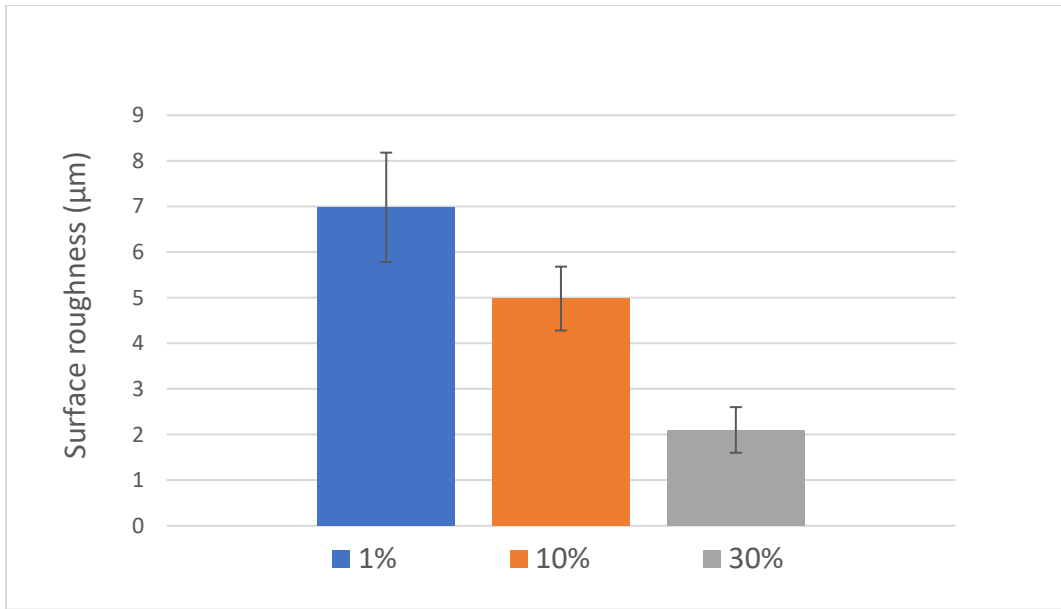
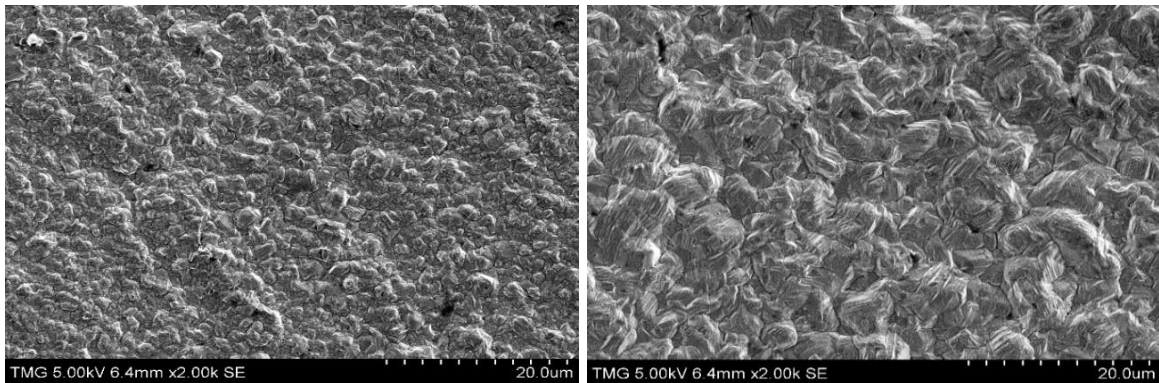


Figure 3-24. The effect of different anodic charge (1%, 10% and 30% of cathodic charge) on the surface roughness of the deposits by keeping the cathodic charge constant at 0.013 C/mm<sup>2</sup> for the total charge of 13.8 C/mm<sup>2</sup>

It is found that by increasing the polishing percentage from 1% to 30% the surface roughness gradually decreases. This is due to the fact that by increasing the material removal (polishing percentage) in each cycle, more defects are being eliminated from the deposit resulting in a smoother surface and consequently less porous depositions are obtained.

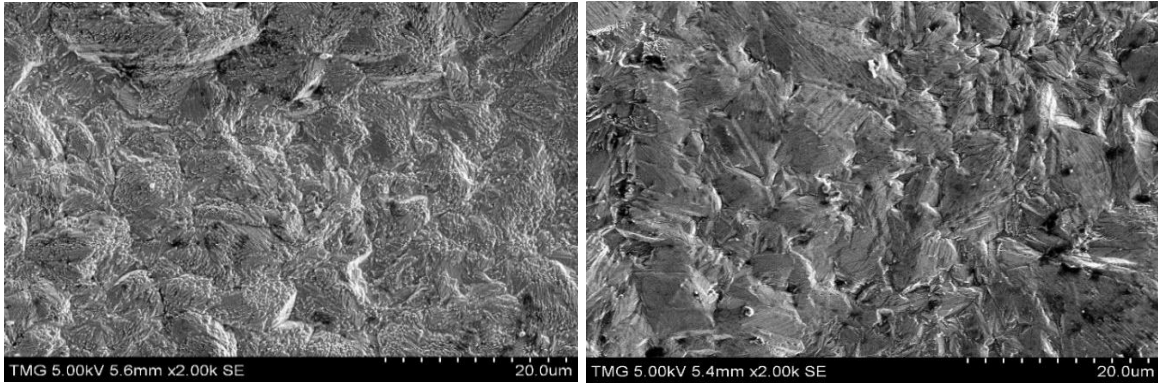
### 3.3.2. The effect of quantity of electricity on the morphology of the pulse plated coatings (polishing pulse charge is 10% of the depositing pulse charge)

Figure 3-25 shows the SEM micrographs of the pulse plated coatings (10% polished deposits) obtained at different quantity of electricity at a cathodic potential of -150 mV and anodic potential of +100 mV.



a) 0.2 C/mm<sup>2</sup> X2000

b) 0.6 C/mm<sup>2</sup> X2000



c) 2.4 C/mm<sup>2</sup> X2000

d) 7.2 C/mm<sup>2</sup> X2000

*Figure 3-25. The SEM micrographs of the pulse plated coatings obtained at the different total quantity of electricity. a)0.24 C/mm<sup>2</sup> X2000 b)0.6 C/mm<sup>2</sup> X2000 c)2.4 C/mm<sup>2</sup> X2000 d)7.2 C/mm<sup>2</sup> X2000*

As it is clear from Figure 3-25, grain growth happens, and nodularity of the grains is reduced by increasing the total charge due to the elimination of the defects during anodic pulse.

### 3.4. Comparison of galvanostatic, potentiostatic and pulse-potentiostatic copper plating

Figure 3-26 compares the surface roughness of the copper deposits in function of charge for three different plating modes at the same time.

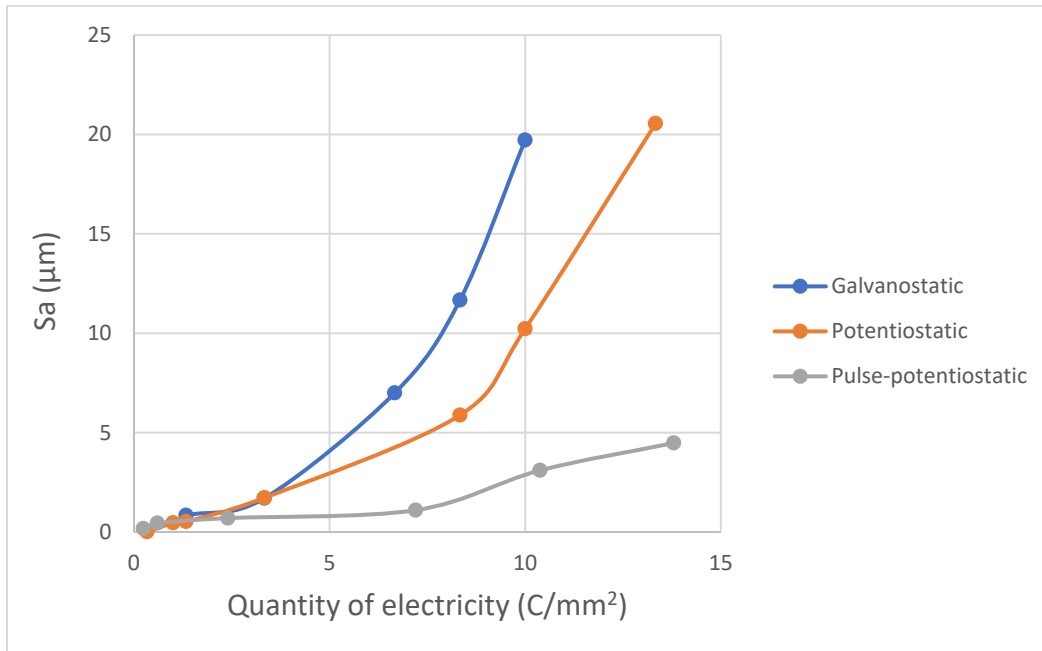


Figure 3-26. The schematic of difference in surface roughness of the copper deposits in function of charge for galvanostatic, potentiostatic and pulse-potentiostatic plating modes

As it is clear, copper deposits get rough in galvanostatic mode sooner than two other plating methods, reaching to 20 μm surface roughness for 10 C/mm<sup>2</sup> charge. However, surface roughness of the copper deposit made by the potentiostatic method is 10 μm, which is two times lower than that for the galvanostatic mode for the same charge.

Moreover, in pulse-potentiostatic plating mode, the surface roughness is only increasing from 0.17 μm to 4.48 μm for the corresponding charges of 0.24 C/mm<sup>2</sup> and 13.8 C/mm<sup>2</sup>.

Differences in plating modes mechanisms cause the different quality of the deposits for a same given charge.

According to the Butler-volmer equation, current density depends on the electrode potential,  $j(\eta)$ , where  $j$  is the current density and  $\eta$  is the activation overpotential which defines as  $E - E_{eq}$ .

Furthermore,  $j(\eta) = i/S$ , where  $i$  is the current (A) and  $S$  is the surface area ( $m^2$ ). Under potentiostatic condition, since the overpotential which is a thermodynamic parameter, is not changing, the process is carried out under steady-state condition, however in galvanostatic condition in order to have a constant current, since the surface area is changing,  $j$  is changing as well which leads to the change in overpotential. That is why the potential is varying under the galvanostatic condition.

In pulse-potentiostatic mode, during the anodic time, positive current eliminates the thickness build up at high current density areas (leveling effect of polishing), and improves the step coverage without pores reaching down to the substrate, however in potentiostatic mode (DC current), a charged layer is formed around the cathode and this layer hinders the ions from reaching to the part [21].

As an example, Figure 3-27 shows the remarkable difference in surface quality of the potentiostatic and pulse-potentiostatic copper plated parts for  $10 C/mm^2$  charge.



*Figure 3-27. Copper deposits made by potentiostatic plating and pulse-potentiostatic plating modes from left to right, for the same charge of  $10 \text{ C/mm}^2$*

It is also noted that the results really depend on the conditions of the experiments and may likely vary. For example, by either applying higher potential in potentiostatic mode or applying less current density in galvanostatic mode, smoother surfaces may be associated with the galvanostatic condition rather than the potentiostatic mode.

### 3.5. Electroless copper plated ABS printed part

Figure 3-28 shows the copper electroless plated ABS part created according to Table 2-1.

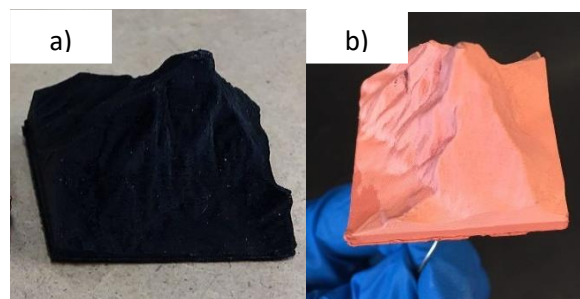


*Figure 3-28. a) ABS printed part b) Electroless plated ABS part*

### 3.5.1. Surface roughness and resistance measurements

Figure 3-29 shows the 2D and 3D maps of the determined location of the ABS printed part.

The obtained surface roughness is  $S_a = 18.27 \pm 0.1 \mu\text{m}$ .

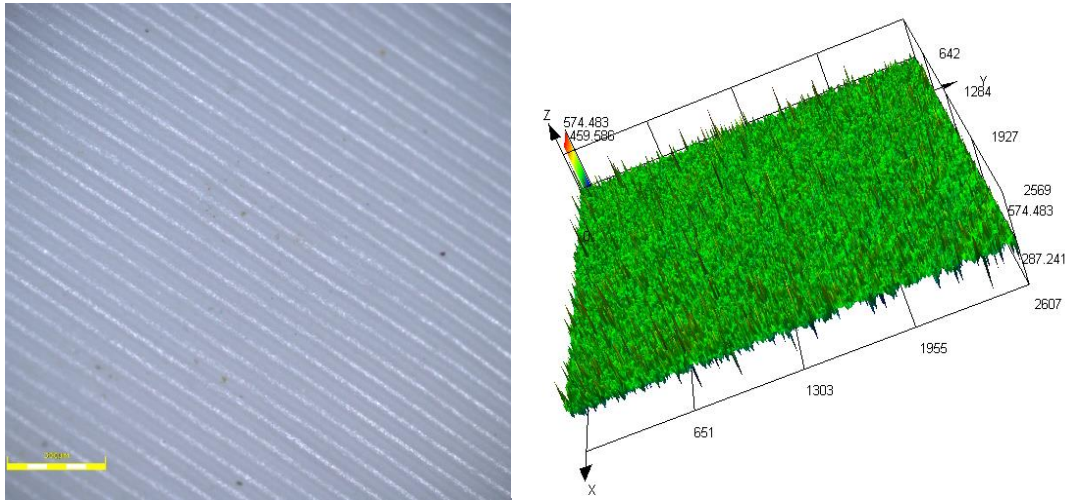


*Figure 3-29. The 2D and 3D maps of the ABS part obtained by confocal laser microscopy*

Note that each layer is approximately  $100 \mu\text{m}$  thickness due to the layer by layer printing.

Figure 3-30 shows the 3D map of the determined location of the ABS part after electroless copper plating. The surface roughness achieved at this condition is  $S_a = 11.13 \pm 0.5 \mu\text{m}$ .

Note that surface roughness decreases after electroless plating.

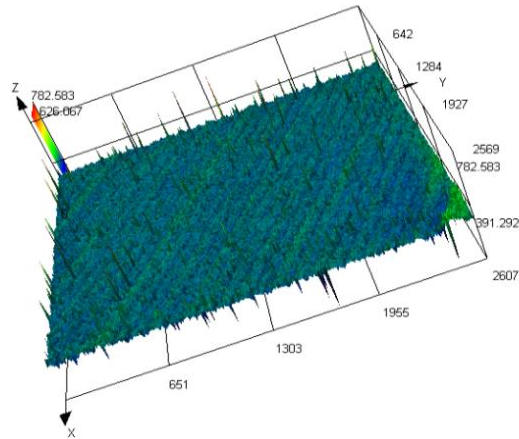


*Figure 3-30. The 3D map of the electroless copper plated ABS part*

0.1 Ohm resistance is also obtained from the electroless copper plated ABS part.

### 3.6. Copper electroforming of ABS printed part in galvanostatic, potentiostatic and pulse-potentiostatic modes

Figure 3-31 shows the electroformed parts of copper electroless plated ABS parts in three different modes. As it is clear, the part produced by the galvanostatic method, is the roughest part due to the non-stationary condition during electroplating ( $E$  is variable). However there is a remarkable reduction in surface roughness of two parts produced by potentiostatic and pulse-reverse potentiostatic modes. It is noted that the thickness build up at high current density areas is eliminated during the anodic pulse improving the surface quality (roughness) [21].

The electroformed part can be either dissolved in acetone to obtain a lightweight metallic part or kept as it is, depending on the applications.



*Figure 3-31. Copper electroforming of a non-conductive 3D printed ABS part **Above)** Right to left: Galvanostatic copper electroformed part, potentiostatic copper electroformed part, pulse-potentiostatic copper electroformed part **Below)** View from inside the hollow part*

### 3.6.1. Surface roughness measurements

Figure 3-32 shows the 3D maps of the morphology of the copper electroplated ABS part for the three conditions, galvanostatic, potentiostatic and pulse-reverse electroplating.

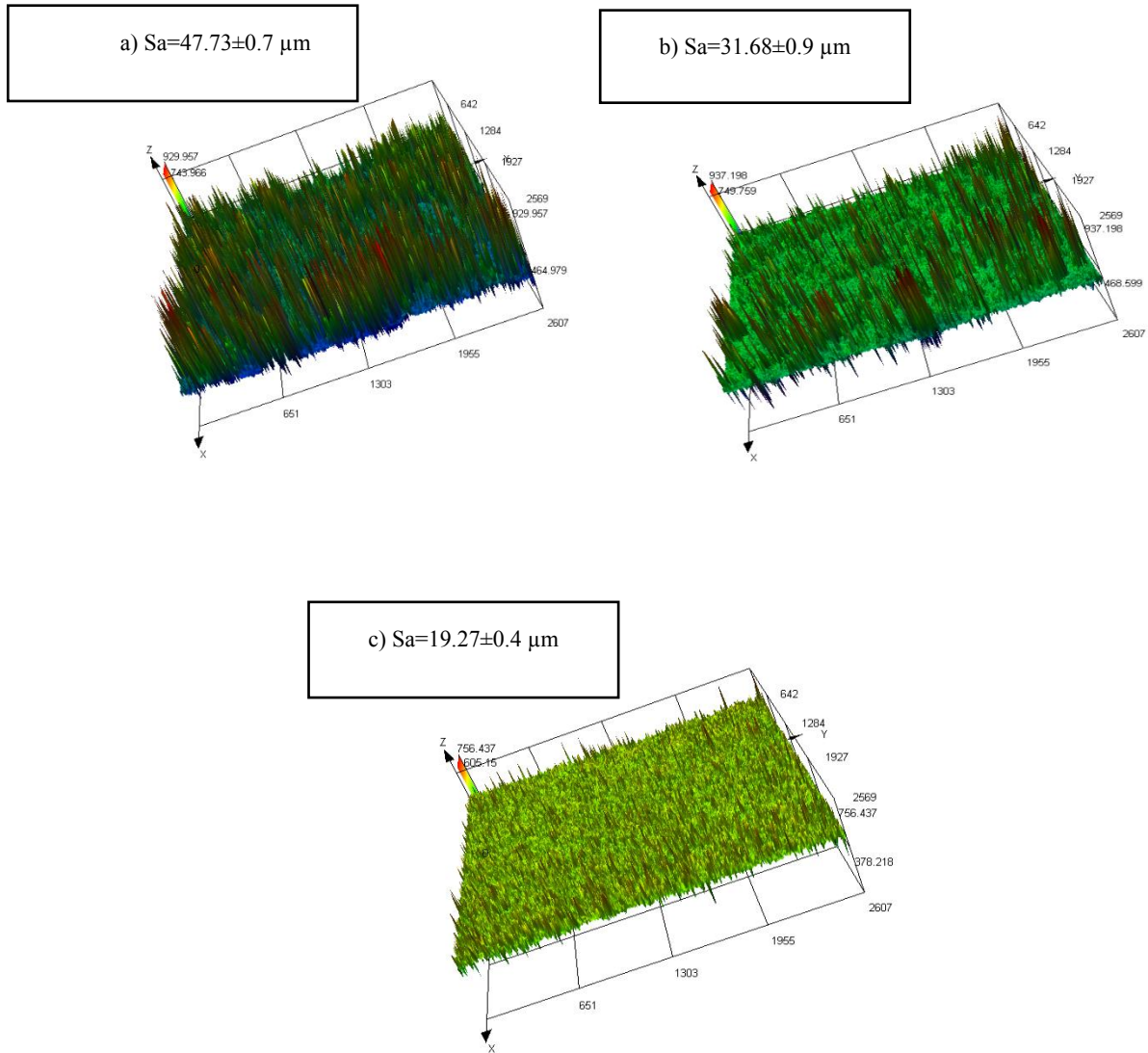
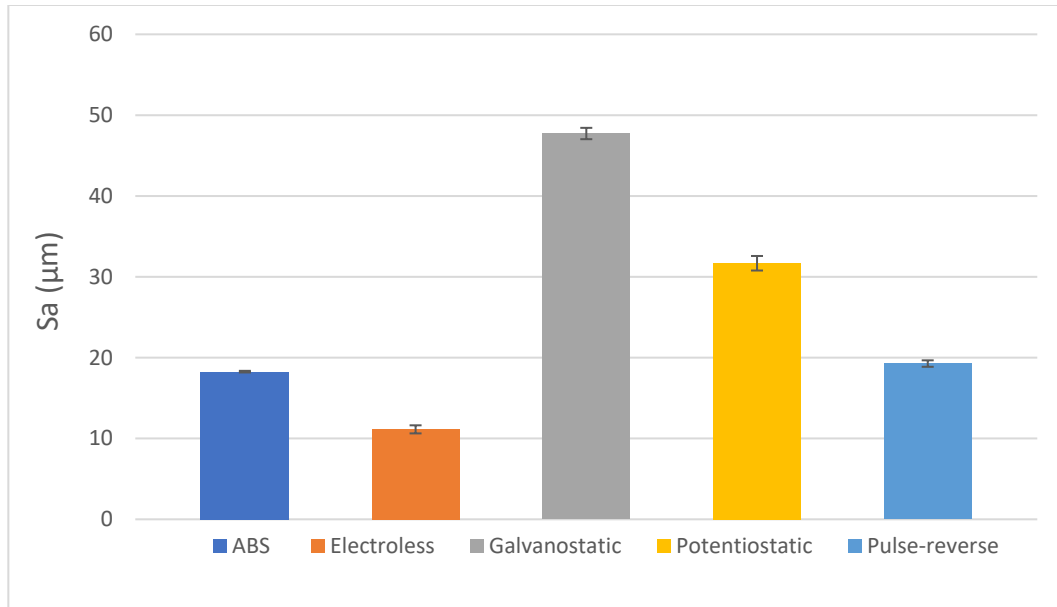


Figure 3-32. 3D maps of the morphology of the copper electroplated ABS part in three conditions: a) Galvanostatic b) Potentiostatic c) Pulse-reverse electroplating

Figure 3-33 compares the surface roughness of the ABS printed part, Electroless plated ABS part, Galvanostatic copper electroplated electroless plated ABS part, Potentiostatic copper electroplated electroless plated ABS part, Pulse-reverse copper electroplated electroless plated ABS part.



*Figure 3-33. Surface roughness comparison of AM part created by different electroplating modes*

As it was expected, the surface roughness of the part after electroless copper plating is decreased which means that it fills the valleys of the surface. Moreover, surface roughness of the pulse plated part is very close to the initial 3D ABS part and is less than that of the two other electroformed parts.

### 3.7. Applications

#### 1) Decorative applications

Electroplating is one of the cost-effective way to make products such as jewelry, statues, etc.

Figure 3-34 and 3-35 show copper electroformed plaster parts made by potentiostatic plating method created for the Art department.



*Figure 3-34. Copper electroformed plaster part (potentiostatic mode, - 0.3V applied potential).*

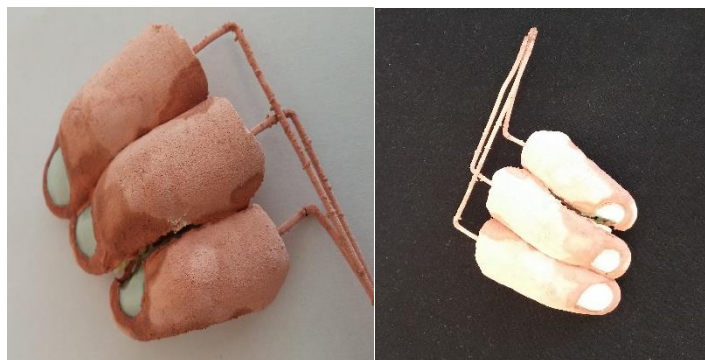


*Figure 3-35. Copper electroformed plaster part*

In the proposed manufacturing method (see Figure 3-36.), 3D polymer part is printed by additive manufacturing technology (AMT) in a first step, then an initial conductive layer is applied in a

second step (electroless plating or applying a conductive paint). Subsequently, metal is deposited onto the part by electroplating until sufficient thickness is obtained. In the last step, the polymer model is removed by dissolving in a solvent.

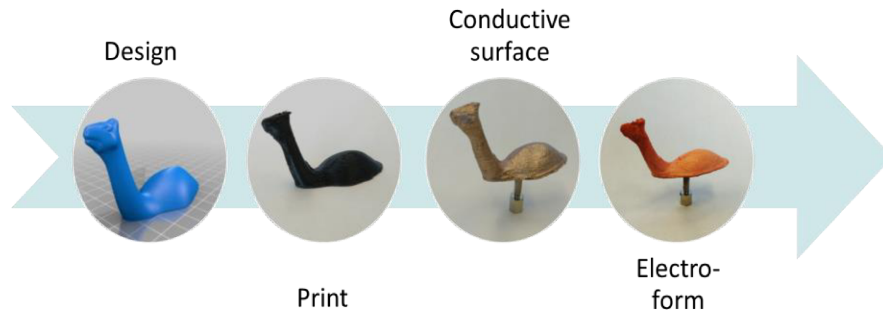


*Figure 3-36. Process flow from 3D printing a non-conductive ABS part up to electroplating (Cu) the copper painted part*

## 2) Electronic chips

Figure 3-37 shows a printed part with SLA printer (resin substrate) which is electroless copper plated.



*Figure 3-37. Copper electroforming of a SLA printed part (electronic chips)*

### 3) Fabrication of electrodes for electropolishing applications

Figure 3-38 shows copper electroplated ABS printed parts.

Sometimes in electropolishing process, the part to be polished has hard-to-reach area which needs a specific electrode to be located inside a part. In this case, a desired ABS part can be copper electroformed to act as an electrode.

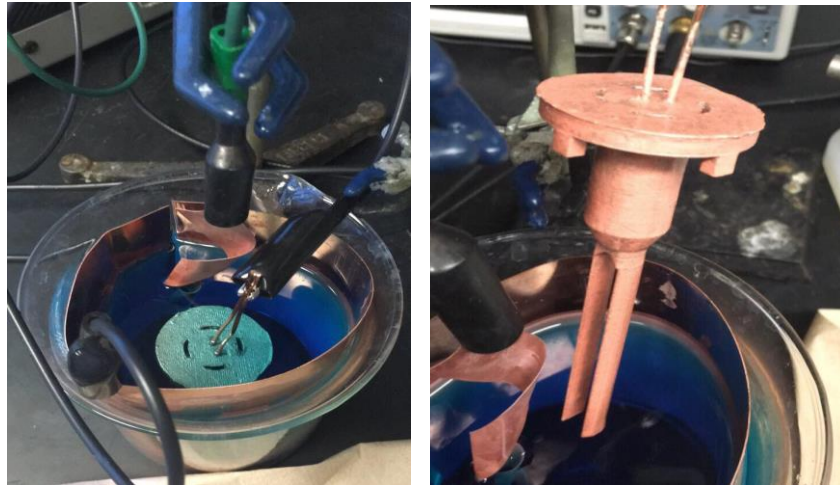


*Figure 3-38. An example of fabrication of an electrode used in electropolishing*

## 4. Conclusion and future work

The first study discussed in this thesis was conducted to evaluate the optimal parameters of copper electroplating in different plating modes for planar geometry with the goal of obtaining the smooth coating as much as possible. In galvanostatic condition, through investigations of surface roughness measurement of the deposits obtained at three different current densities (5, 10, 15 mA/Cm<sup>2</sup>), 5 mA/Cm<sup>2</sup> has been chosen due to the lowest surface roughness of the coating. Moreover, through investigation of surface roughness measurement and SEM images of the coated samples at 5 mA/Cm<sup>2</sup>, the columnar structure was observed in which by increasing the quantity of electricity, the V-shaped grains starts to grow, and surface roughness is also increasing significantly.

In potentiostatic condition, through investigations of the polarization experiment, surface roughness measurements and SEM characterization of the same charged coatings at different potentials, -150 mV has been chosen as the optimal electroplating potential. It is noticeable that due to the more stability of the process, smoother surfaces can be achieved compared to that of galvanostatic condition.

Pulse-potentiostatic plating helped to improve the surface quality of the coatings. It can be found from pulse-electroplated samples that even much smoother surfaces are obtained due to the polishing steps during the plating which leads to eliminate the surface defects. Importantly, it was found that by increasing the quantity of electricity, the surface roughness is increasing only slightly.

In the second study discussed in this work resulted to evaluate the electroplated coatings on ABS parts in different plating modes using the obtained optimal parameters. It was observed that The

surface roughness of the ABS part was reduced after electroless plating and increased after electroforming. Less increase of surface roughness was observed in the pulse-plated 3D parts compared to other plating methods.

Recommendations for future research are summarized below:

- 1) Since using formaldehyde as a reducing agent in electroless copper plating is accompanied by the hydrogen evolution, alloying copper with different metals has a pronounced effect during anodic oxidation of formaldehyde.
- 2) Evaluate the influence of different parameters such as temperature, agitation, pulse parameters and concentration of copper deposition electrolyte on quality of the produced coating and mechanical properties.
- 3) Investigate the effect of different AM part with different geometry and material on the coating properties.
- 4) Investigate the effect of alloying copper on the surface quality and mechanical properties of the coating.
- 5) Evaluate the effect of geometry of the workpiece on the thickness distribution of the deposit over the sample.

## References

- [1] H. Y. Cheh, "Electrodeposition of Gold by Pulsed Current," *J. Electrochem. Soc.*, vol. 118, no. 4, pp. 551–557, 1971.
- [2] O. Chène and D. Landolt, "The influence of mass transport on the deposit morphology and the current efficiency in pulse plating of copper," *J. Appl. Electrochem.*, vol. 19, no. 2, pp. 188–194, 1989.
- [3] D. Zhu, N. S. Qu, and K. C. Chan, "Development of joint electroforming technology," *J. Mater. Process. Technol.*, vol. 63, no. 1–3, pp. 844–847, 1997.
- [4] C. C. Hu and C. M. Wu, "Effects of deposition modes on the microstructure of copper deposits from an acidic sulfate bath," *Surf. Coatings Technol.*, vol. 176, no. 1, pp. 75–83, 2003.
- [5] T. Gupta, *Copper interconnect technology*. 2009.
- [6] R. Island, "ELECTROLESS ( Autocatalytic , Chemical ) PLATING by Jim Henry."
- [7] I. Ohno, "Electrochemistry of electroless plating," *Mater. Sci. Eng. A*, vol. 146, no. 1–2, pp. 33–49, 1991.
- [8] A. Garcia *et al.*, "ABS polymer electroless plating through a one-step poly(acrylic acid) covalent grafting," *ACS Appl. Mater. Interfaces*, vol. 2, no. 4, pp. 1177–1183, 2010.
- [9] F. Wang, S. Arai, and M. Endo, "Metallization of multi-walled carbon nanotubes with copper by an electroless deposition process," *Electrochem. commun.*, vol. 6, no. 10, pp. 1042–1044, 2004.
- [10] J. B. H. Glenn O. Mallory, *Electroless Plating: Fundamentals and Applications*. William Andrew, 1990.
- [11] M. Schlesinger and M. Paunovic, *Modern Electroplating: Fifth Edition*. 2011.
- [12] K. Yamagishi, N. Okamoto, N. Mitsumata, N. Fukumuro, S. Yae, and H. Matsuda, "Reaction process of two-step Catalysation Pre-treatment for Electroless Plating on Non-conducting Substrates," *Trans. Inst. Met. Finish.*, vol. 82, no. 3–4, 2004.

- [13] P. Bindra, "Mechanisms of Electroless Metal Plating," *J. Electrochem. Soc.*, vol. 130, no. 11, p. 1112, 1983.
- [14] J. J. Kim and S. K. Kim, "Optimized surface pretreatments for copper electroplating," *Appl. Surf. Sci.*, vol. 183, no. 3–4, pp. 311–318, 2001.
- [15] A. Fava *et al.*, "Characterization of Thick Film of Copper Electrodeposited for Cryogenic Applications," *J. Electrochem. Soc.*, vol. 161, no. 10, pp. D540–D545, 2014.
- [16] W. C. Gau *et al.*, "Copper electroplating for future ultralarge scale integration interconnection," *J. Vac. Sci. Technol. A Vacuum, Surfaces, Film.*, vol. 18, no. 2, p. 656, 2000.
- [17] J. O. Bockris and A. K. N. Reddy, *Modern Electrochemistry: An introduction to an interdisciplinary area Vol. 2*, vol. 1. 2015.
- [18] N. Kanani, *Electroplating: Basic Principles, Processes and Practice*. 2005.
- [19] E. T. McAdams, A. Lacknermeier, J. A. McLaughlin, D. Macken, and J. Jossinet, "The linear and non-linear electrical properties of the electrode-electrolyte interface," *Biosens. Bioelectron.*, vol. 10, no. 1–2, pp. 67–74, 1995.
- [20] C. H. Hamann, A. Hamnett, and W. Vielstich, *Electrochemistry*. 2007.
- [21] M. S. Chandrasekar and M. Pushpavanam, "Pulse and pulse reverse plating-Conceptual, advantages and applications," *Electrochimica Acta*, vol. 53, no. 8. pp. 3313–3322, 2008.
- [22] N. V. Mandich, "Pulse and pulse-reverse electroplating," *Metal Finishing*, vol. 100, no. 1 SUPPL. pp. 359–364, 2002.
- [23] K. M. Yin and S. L. Jan, "Experimental study of pulse with reverse platings on nickel-iron alloys from sulphate solutions," *Trans. Inst. Met. Finish.*, vol. 74, no. 2, pp. 51–54, 1996.
- [24] D. L. Grimmitt, "A Comparison of DC and Pulsed Fe-Ni Alloy Deposits," *J. Electrochem. Soc.*, vol. 140, no. 4, p. 973, 1993.
- [25] W. Kim and R. Weil, "Property enhancement of nickel electrodeposits by anodic current pulses," *Surf. Coatings Technol.*, vol. 31, no. 2, pp. 143–150, 1987.

- [26] P. F. Mentone, "Pulse vs. DC plating," *Metal Finishing*, vol. 103, no. 6. pp. 14–18, 2005.
- [27] P. Leisner, M. Fredenberg, and I. Belov, "Pulse and pulse reverse plating of copper from acid sulphate solutions," *Trans. Inst. Met. Finish.*, vol. 88, no. 5, pp. 243–247, 2010.
- [28] L. M. Chang, "Diffusion layer model for pulse reverse plating," *Journal of Alloys and Compounds*, vol. 466, no. 1–2. 2008.
- [29] N. Tantavichet and M. D. Pritzker, "Effect of plating mode, thiourea and chloride on the morphology of copper deposits produced in acidic sulphate solutions," *Electrochim. Acta*, vol. 50, no. 9, pp. 1849–1861, 2005.
- [30] W. C. Tsai, C. C. Wan, and Y. Y. Wang, "Mechanism of copper electrodeposition by pulse current and its relation to current efficiency," *J. Appl. Electrochem.*, vol. 32, no. 12, pp. 1371–1378, 2002.
- [31] B. Vayre, F. Vignat, and F. Villeneuve, "Designing for additive manufacturing," in *Procedia CIRP*, 2012, vol. 3, no. 1, pp. 632–637.
- [32] ASTM, "ASTM F2792 - 12a. Standard Terminology for Additive Manufacturing Technologies," *ASTM F2792-10e1*. pp. 2–4, 2013.
- [33] S. H. Huang, P. Liu, A. Mokasdar, and L. Hou, "Additive manufacturing and its societal impact: A literature review," *International Journal of Advanced Manufacturing Technology*, vol. 67, no. 5–8. pp. 1191–1203, 2013.
- [34] E. Herderick, "Additive manufacturing of metals: A review," *Mater. Sci. Technol. Conf. Exhib. 2011, MS T'11*, vol. 2, no. 176252, pp. 1413–1425, 2011.
- [35] K. V. Wong and A. Hernandez, "A Review of Additive Manufacturing," *ISRN Mech. Eng.*, vol. 2012, pp. 1–10, 2012.
- [36] J. P. Kruth, M. C. Leu, and T. Nakagawa, "Progress in additive manufacturing and rapid prototyping," *CIRP Ann. - Manuf. Technol.*, vol. 47, no. 2, pp. 525–540, 1998.
- [37] Q. Zhou, J. Panetta, and D. Zorin, "Worst-case structural analysis," *ACM Trans. Graph.*, vol. 32, no. 4, p. 1, 2013.
- [38] E. Mikolajewska, M. Macko, L. Ziarniecki, S. Stanczak, P. Kawalec, and D. Mikolajewski,

- “3D printing technologies in rehabilitation engineering,” *J. Heal. Sci.*, vol. 4, no. 12, pp. 78–83, 2014.
- [39] A. Ambrosi and M. Pumera, “3D-printing technologies for electrochemical applications,” *Chem. Soc. Rev.*, vol. 45, no. 10, pp. 2740–2755, 2016.
- [40] J. Kietzmann, L. Pitt, and P. Berthon, “Disruptions, decisions, and destinations: Enter the age of 3-D printing and additive manufacturing,” *Business Horizons*, vol. 58, no. 2, pp. 209–215, 2015.
- [41] S. S. Crump, “Apparatus and Method for Creating Three-Dimensional Objects,” *US Pat. 5,121,329*, p. 15, 1992.
- [42] K. G. Cooper, *Rapid Prototyping Technology: Selection and Application*. 2001.
- [43] J. P. Kruth, “Material Incess Manufacturing by Rapid Prototyping Techniques,” *CIRP Ann. - Manuf. Technol.*, vol. 40, no. 2, pp. 603–614, 1991.
- [44] K. U. Bletzinger and E. Ramm, “Structural optimization and form finding of light weight structures,” *Comput. Struct.*, vol. 79, no. 22–25, pp. 2053–2062, 2001.
- [45] V. K. Balla, S. Bose, and A. Bandyopadhyay, “Processing of bulk alumina ceramics using laser engineered net shaping,” *Int. J. Appl. Ceram. Technol.*, vol. 5, no. 3, pp. 234–242, 2008.
- [46] Y. S. Liao, H. C. Li, and Y. Y. Chiu, “Study of laminated object manufacturing with separately applied heating and pressing,” *Int. J. Adv. Manuf. Technol.*, vol. 27, no. 7–8, pp. 703–707, 2006.
- [47] B. Vaupotič, M. Brezočnik, and J. Balič, “Use of PolyJet technology in manufacture of new product,” *J. Achiev. Mater. Manuf. Eng.*, vol. 18, no. 1, pp. 319–322, 2006.
- [48] R. Singh, “Process capability study of polyjet printing for plastic components,” *Evol. Ecol.*, vol. 25, no. 4, pp. 1011–1015, 2011.
- [49] R. Van Noort, “The future of dental devices is digital,” *Dent. Mater.*, vol. 28, no. 1, pp. 3–12, 2012.
- [50] S. J. Hollister, “Porous scaffold design for tissue engineering,” *Nature Materials*, vol. 4,

- no. 7. pp. 518–524, 2005.
- [51] R. Makovec, “Digital technologies in dental laboratories ,” *The 3rd International Conference on Additive Technologies; DAAAM Specialized Conference*. pp. 1–2, 2010.
- [52] I. Gibson, T. Kvan, and L. Wai Ming, “Rapid prototyping for architectural models,” *Rapid Prototyp. J.*, vol. 8, no. 2, pp. 91–95, 2002.
- [53] T. Wohlers, “Making Products By Using Additive Manufacturing,” *Manuf. Eng.*, vol. 146, no. 4, pp. 70-74-77, 2011.
- [54] F. E. Stone, “Electroless Copper In Printed Wiring Board Fabrication,” *Electroless Plat. Fundamentals Appl.*, pp. 331–369, 1990.
- [55] N. D. Nikolić, K. I. Popov, L. J. Pavlović, and M. G. Pavlović, “Morphologies of copper deposits obtained by the electrodeposition at high overpotentials,” *Surf. Coatings Technol.*, vol. 201, no. 3–4, pp. 560–566, 2006.
- [56] N. D. Nikolić, K. I. Popov, L. J. Pavlović, and M. G. Pavlović, “The effect of hydrogen codeposition on the morphology of copper electrodeposits. I. the concept of effective overpotential,” *J. Electroanal. Chem.*, vol. 588, no. 1, pp. 88–98, 2006.
- [57] N. D. Nikolić, G. Branković, M. G. Pavlović, and K. I. Popov, “The effect of hydrogen co-deposition on the morphology of copper electrodeposits. II. Correlation between the properties of electrolytic solutions and the quantity of evolved hydrogen,” *J. Electroanal. Chem.*, vol. 621, no. 1, pp. 13–21, 2008.
- [58] M. Adamik, P. . Barna, and I. Tomov, “Columnar structures in polycrystalline thin films developed by competitive growth,” *Thin Solid Films*, vol. 317, no. 1–2, pp. 64–68, 1998.
- [59] A. M. Lafront, B. Veilleux, and E. Ghali, “Galvanostatic and microscopic studies of nodulation during copper electrolysis,” *J. Appl. Electrochem.*, vol. 32, no. 3, pp. 329–337, 2002.
- [60] A. Milchev and M. Irene Montenegro, “A galvanostatic study of electrochemical nucleation,” *J. Electroanal. Chem.*, vol. 333, no. 1–2, pp. 93–102, 1992.